Continuum Mech. Thermodyn. (2022) 34:781–827
https://doi.org/10.1007/s00161-022-01090-y

ORIGINAL ARTICLE

Hossein B. Khaniki · Mergen H. Ghayesh · Rey Chin · Shahid Hussain

Nonlinear continuum mechanics of thick hyperelastic sandwich beams using various shear deformable beam theories

Received: 22 September 2021 / Accepted: 1 February 2022 / Published online: 9 March 2022

Abstract In this study, the time-dependent mechanics of multilayered thick hyperelastic beams are investigated for the first time using five different types of shear deformation models for modelling the beam (i.e. the Euler–Bernoulli, Timoshenko, third-order, trigonometric and exponential shear deformable models), together with the von Kármán geometrical nonlinearity and Mooney–Rivlin hyperelastic strain energy density. The laminated hyperelastic beam is assumed to be resting on a nonlinear foundation and undergoing a time-dependent external force. The coupled highly nonlinear hyperelastic equations of motion are obtained by considering the longitudinal, transverse and rotation motions and are solved using a dynamic equilibrium technique. Both the linear and nonlinear time-dependent mechanics of the structure are analysed for clamped–clamped and pinned–pinned boundaries, and the impact of considering the shear effect using different shear deformation theories is discussed in detail. The influence of layering, each layer's thickness, hyperelastic material positioning and many other parameters on the nonlinear frequency response is analysed, and it is shown that the resonance position, maximum amplitude, coupled motion and natural frequencies vary significantly for various hyperelastic and layer properties. The results of this study should be useful when studying layered soft structures, such as multilayer plastic packaging and laminated tubes, as well as modelling layered soft tissues.

Keywords Layered beams · Soft beams · Hyperelastic beams · Nonlinear vibration · Nonlinear dynamics · Laminated beams · Multilayered beams · Sandwich beams

1 Introduction

Layering structures is an effective method for optimising their mechanical, physical and electrical properties for a specific purpose. For instance, in the automotive industry, reducing the weight of the structure and increasing the stiffness lead to significant environmental benefits (lowering the fuel consumption and increasing automobile's performance [1,2]) which is made feasible by fabricating multilayered parts.

Communicated by Andreas Öchsner.

H. B. Khaniki (✉) · M. H. Ghayesh (✉) · R. Chin
School of Mechanical Engineering, University of Adelaide, Adelaide, SA 5005, Australia
E-mail: hossein.bakhshikhaniki@adelaide.edu

M. H. Ghayesh
E-mail: mergen.ghayesh@adelaide.edu.au

S. Hussain
Faculty of Science and Technology, University of Canberra, Canberra, Australia

In many engineering applications, structures are fabricated with three layers (e.g. in laminated packaging); the outer layers are called the skins (upper skin and lower skin) and the middle layer is the core. If the purpose of the design is to increase the strength against bending loads, the core is usually made of a softer material with a higher thickness and the outer skins are thinner and stiffer. If the structure is used in an uncertain environment, the outer skins are made of softer materials to propagate the force throughout the structure and avoid cracks in a brittle core. In some other engineering structures, researchers gradually change the material properties to fabricate functionally graded structures which have been studied in Refs. [3–6].

Over the past few years, researchers have analysed different layered *elastic (versus hyperelastic in this paper)* structures to understand their mechanical behaviour under diverse conditions. A brief review of previous studies in this field is given in this section; however, interested readers seeking a more detailed literature review are referred to Refs. [7–10].

For bending analysis of layered *elastic* beams [11,12], researchers have used different beam theories and analysed layered beam structures. By neglecting the shear effects, Chai and Yap [13] examined the bending behaviour of layered composite structures using classic beam theory (CBT). By comparing the results with those of a finite element modelling (FEM), it was shown that the coupling terms between the layers play a significant role in predicting the mechanical behaviour accurately. Chen et al [14] added the shear influence to the model using the first-order shear deformable beam theory; it was shown that the bending deformation of the Timoshenko beam model is higher than the CBT and the difference is higher for any lower thickness-to-length ratio. Özütok and Madenci [15] used a higher-order shear deformation theory together with FEM for timed-independent analysis of layered composite beams and verified the results by comparing them with those available in the literature.

For *linear* vibration analysis of layered *elastic* beams [16–18], Emam and Nayfeh [19] investigated the free vibration of layered composites using the Euler–Bernoulli beam theory. The axial motion was considered in the formulation and was substituted in the transverse equation of motion. Natural frequencies were obtained for different axial loads and boundary conditions; it was reported that for the studied six-layer beam model, the layer positioning has a significant effect in varying the fundamental frequency for different axial loads. A first-order shear deformable beam theory was used by Banerjee and Sobey [20] to examine the free oscillation of laminated structures under axial loading. A closed-form analytical solution was presented showing accuracy in predicting the natural frequencies and mode shapes of layered beams. Damanpack and Khalili [21] used higher-order beam theory to model the longitudinal–transverse coupled motion of layered structures. Hamilton's principle was used to reach the equations of motion showing that the natural frequencies obtained from this model agree with the experimental results presented in Ref. [22].

For *nonlinear* vibration analysis of *elastic* beams, Zhang et al. [23] studied the nonlinear forced oscillation of laminated beams in a humid thermal condition. Only the transverse motion was considered in the formulation, and a nonlinear energy sink was added to the model. The equations of motion were solved using a fourth-order Rung–Kutta (RK4) method and a two-term harmonic balance (HB) scheme. It was shown that the nonlinear studied model has a hardening behaviour and adding a nonlinear energy sink can reduce the maximum amplitude of the transverse vibration significantly. Shen et al. [24] examined the nonlinear free oscillation behaviour of layered graphene-strengthened beams; Halpin–Tsai model was employed to predict the physical properties of the combination of the matrix and fibres. A higher-order shear deformable theory, together with the von-Kármán geometrical nonlinearity, was used to model the beam. By employing a two-step perturbation technique, it was shown that the layering and positioning of fibres has a significant effect in varying the nonlinear frequency ratio and the natural frequencies. Three-layered and bi-layered shear deformable *elastic* beams have been studied by Ghayesh et al. [25]; it was shown that the resonance region change based on the layer sorting and both hardening and softening behaviour can be observed while considering geometrical imperfections. Other types of layered structures have also been examined by researchers, and interested authors are referred to Refs. [26,27] for more information about layered-plate and layered-shell structures focused investigations.

The previously mentioned studies focus on *elastic* structures that undergo small strains while facing different types of loadings; even the nonlinear ones are based on *geometric* nonlinearities and small strains. Soft structures cannot be modelled as a linear elastic material and require more accurate hyperelastic assumptions and formulations; in other words, a *material* nonlinearity should be taken into account, as done in this paper.

Multilayered *hyper*elastic structures have been used widely in many products. For instance, multilayer plastic packaging is used for packaging different products, such as food packaging which has been a trending topic over the last few years in waste management, recycling and optimised packaging [28–31]. Furthermore, human body organs act as hyperelastic components and many parts are made of different layers, such as the artery, which is made of three hyperelastic layers (intima, media and adventitia) [32].

Previously, axially moving hyperelastic structures and porous-hyperelastic structures have been investigated by Khaniki et al. [33,34]; however, until now, there have been no studies on the time-dependent mechanics of layered hyperelastic structures. In this study, a comprehensive analysis of the mechanics of multilayered thick hyperelastic structures is presented for the first time as having different boundary conditions via different shear theories. Large strain modelling, together with large-amplitude displacements, is modelled using the Mooney–Rivlin strain energy model (for material nonlinearity) and the von Kármán geometrical nonlinearity. Different types of shear deformable beam theories (Euler–Bernoulli, Timoshenko, third-order, trigonometric and exponential shear deformable models) are used to model the layered structures and the influence of layering, material positioning and the thickness of the core and skins is discussed in detail.

2 Layered hyperelastic shear deformable beam formulation

For a thick-layered shear deformable beam (Fig. 1), considering the plane motion, the axial and transverse deformations are written as [35]

$$u(x,z,t) = \chi(z)\, w_x(x,t) - \chi(z)\,\phi(x,t) + u(x,t) - z w_x(x,t), \tag{1}$$

$$w(x,z,t) = w(x,t), \tag{2}$$

where u and w are the axial and transverse displacements in the x and z directions (Fig. 1), respectively, subscript x indicates derivations with respect to x, ϕ is the rotation and $\chi(z)$ is the higher-order shear function, which the definition depends on the shear deformable theory used. In this study, five different definitions for $\chi(z)$ are used, which are defined as [36–39]

$$\text{Case 1 (Euler}-\text{Bernoulli beam theory)}: \quad \chi(z) = 0, \tag{3}$$

$$\text{Case 2 (Timoshenko beam theory)}: \quad \chi(z) = z, \tag{4}$$

$$\text{Case 3 (Third}-\text{order beam theory)}: \quad \chi(z) = z\left(1 - \frac{4}{3}\frac{z^2}{h^2}\right), \tag{5}$$

$$\text{Case 4 (Exponential beam theory)}: \quad \chi(z) = z e^{-2(z/h)^2}, \tag{6}$$

$$\text{Case 5 (Trigonometric beam theory)}: \quad \chi(z) = \frac{h}{\pi}\sin\left(\frac{\pi z}{h}\right), \tag{7}$$

where Case 1 indicates that the shear deformation effect is neglected, following the Euler–Bernoulli beam assumption (classic beam theory) when the rotary inertia is also neglected; the advantage of using this model is that the model is simplified by neglecting the rotational degree of freedom by only considering axial and transverse motions. Case 2 defines a linearly varying shear deformation through the thickness of the beam, which represents the Timoshenko beam theory. In this model, the transverse normal plates do not necessarily remain perpendicular (to the mid-surface) after deformation leading to an extra degree of freedom for the rotary inertia. Case 3 shows the shear deformation using a higher-order model following the third-order shear deformable beam theory [36,37]. In this model, the transverse shear stress in the Cases 4 and 5 defines the shear deformation of the beam using an exponential [38] and trigonometric [39] functions, which follow the beam theories of exponential shear deformable and trigonometric, respectively. For all the five cases, the strains are written as

$$\varepsilon_{xx}(x,y,t) = u_x(x,t) - z w_{xx}(x,t) + \chi(z)\, w_{xx}(x,t) - \chi(z)\,\phi_x(x,t) + \frac{1}{2} {w_x}^2(x,t), \tag{8}$$

$$\gamma_{xz}(x,y,t) = 2\varepsilon_{xz}(x,y,t) = \chi_z(z)\, w_x(x,t) - \chi_z(z)\,\phi(x,t), \tag{9}$$

$$\varepsilon_{zz} \neq 0, \tag{10}$$

where ε_{xx} is the axial strain, γ_{xz} is the shear strain and ε_{zz} is the transverse strain that is not equal to zero and should satisfy the incompressibility condition of hyperelastic structures. The deformation gradient (F) is given in Refs. [33,40] which can be used for defining the left Cauchy–Green strain tensor (C) for planar motion as

$$C = F^T F = \begin{bmatrix} (1+\varepsilon_{xx})^2 + {\varepsilon_{xz}}^2 & 0 & \varepsilon_{xz}(2+\varepsilon_{xx}+\varepsilon_{zz}) \\ 0 & 1 & 0 \\ \varepsilon_{xz}(2+\varepsilon_{xx}+\varepsilon_{zz}) & 0 & (1+\varepsilon_{zz})^2 + {\varepsilon_{xz}}^2 \end{bmatrix}, \tag{11}$$

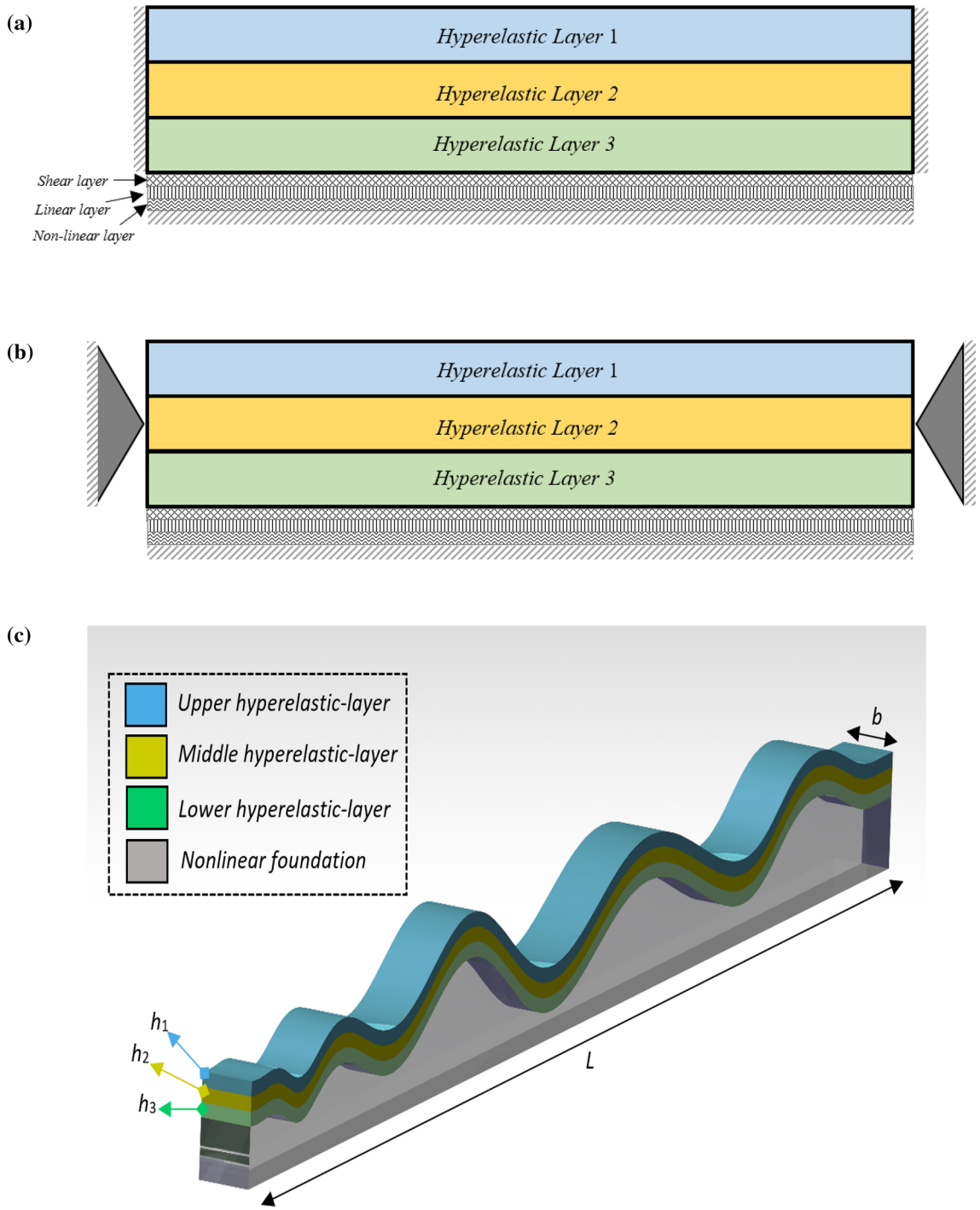

Fig. 1 Schematics of three-layered hyperelastic beam with (**a**) fixed and (**b**) simply supported boundary conditions and (**c**) layer characteristics

where the higher-order strain terms are due to the soft behaviour of hyperelastic materials, which undergo large strains and cannot be ignored. The strain term ε_{zz} can be obtained as a function of ε_{zz} and ε_{zz} by considering $\det(C) = 0$ (the incompressibility condition). For linear elastic models, by neglecting the higher-order strain terms, the Cauchy–Green strain tensor will be [27]

$$C = F^T F = \begin{bmatrix} 1+2\varepsilon_x & 0 & 2\varepsilon_{xz} \\ 0 & 1 & 0 \\ 2\varepsilon_{xz} & 0 & 1+2\varepsilon_z \end{bmatrix}, \tag{12}$$

which is equal to the elastic material strain tensor model. By using the Mooney–Rivlin hyperelastic strain energy density model [41,42], the variation of the total potential energy of the system is written as

$$\begin{aligned} \delta U = \int_0^L \int_A & \left[U_1(x,z)\,\delta u_x(x,t) + U_2(x,z)\,\delta w_x(x,t) \right. \\ & \left. + U_3(x,z)\,\delta w_{xx}(x,t) + U_4(x,z)\,\delta\phi(x,t) + U_5(x,z)\,\delta\phi_x(x,t) \right] \mathrm{d}A\mathrm{d}x, \end{aligned} \tag{13}$$

where

$$\begin{aligned} U_1(x,z) = {} & 8C_T u_x(x,t) + 8C_T[\chi(z) - z]\,w_{xx}(x,t) + 4C_T {w_x}^2(x,t) - 8C_T\chi(z)\,\phi_x(x,t) \\ & - 12C_T {u_x}^2(x,t) - 24C_T[\chi(z) - z]\,u_x(x,t)\,w_{xx}(x,t) + 24C_T\chi(z)\,u_x(x,t)\,\phi_x(x,t) \\ & - 12C_T u_x(x,t)\,{w_x}^2(x,t) - 12C_T[\chi(z) - z]^2 {w_{xx}}^2(x,t) + 12C_T\chi(z)\,{w_x}^2(x,t)\,\phi_x(x,t) \\ & + 24C_T\chi(z)[\chi(z) - z]\,w_{xx}(x,t)\,\phi_x(x,t) - 12C_T[\chi(z) - z]\,{w_x}^2(x,t)\,w_{xx}(x,t) \\ & - 3C_T {w_x}^4(x,t) - 12C_T\chi(z)^2 {\phi_x}^2(x,t) - C_T {\chi_z}^2(z)\,{w_x}^2(x,t) \\ & + 2C_T {\chi_z}^2(z)\,w_x(x,t)\,\phi(x,t) - C_T {\chi_z}^2(z)\,\phi^2(x,t), \end{aligned} \tag{14}$$

$$\begin{aligned} U_2(x,z) = {} & 8C_T u_x(x,t)\,w_x(x,t) + 8C_T[\chi(z) - z]\,w_x(x,t)\,w_{xx}(x,t) + 4C_T {w_x}^3(x,t) \\ & - 8C_T\chi(z)\,w_x(x,t)\,\phi_x(x,t) - 12C_T {u_x}^2(x,t)\,w_x(x,t) \\ & - 24C_T[\chi(z) - z]\,u_x(x,t)\,w_x(x,t)\,w_{xx}(x,t) + 24C_T\chi(z)\,u_x(x,t)\,w_x(x,t)\,\phi_x(x,t) \\ & - 12C_T u_x(x,t)\,{w_x}^3(x,t) - 12C_T[\chi(z) - z]^2 w_x(x,t)\,{w_{xx}}^2(x,t) \\ & + 24C_T\chi(z)[\chi(z) - z]\,w_x(x,t)\,w_{xx}(x,t)\,\phi_x(x,t) + 12C_T\chi(z)\,{w_x}^3(x,t)\,\phi_x(x,t) \\ & - 12C_T[\chi(z) - z]\,{w_x}^3(x,t)\,w_{xx}(x,t) - 3C_T {w_x}^5(x,t) - 12C_T\chi(z)^2 w_x(x,t)\,{\phi_x}^2(x,t) \\ & - C_T {\chi_z}^2(z)\,{w_x}^3(x,t) + 2C_T {\chi_z}^2(z)\,{w_x}^2(x,t)\,\phi(x,t) - C_T {\chi_z}^2(z)\,w_x(x,t)\,\phi^2(x,t) \\ & + 2C_T {\chi_z}^2(z)\,w_x(x,t) - 2C_T {\chi_z}^2(z)\,\phi(x,t) - 2C_T {\chi_z}^2(z)\,u_x(x,t)\,w_x(x,t) \\ & + 2C_T {\chi_z}^2(z)\,u_x(x,t)\,\phi(x,t) - 2C_T {\chi_z}^2(z)[\chi(z) - z]\,w_x(x,t)\,w_{xx}(x,t) \\ & - C_T {\chi_z}^2(z)\,{w_x}^3(x,t) + 2C_T {\chi_z}^2(z)\,\chi(z)\,w_x(x,t)\,\phi_x(x,t) \\ & + 2C_T {\chi_z}^2(z)[\chi(z) - z]\,w_{xx}(x,t)\,\phi(x,t) + C_T {\chi_z}^2(z)\,{w_x}^2(x,t)\,\phi(x,t) \\ & - 2C_T {\chi_z}^2(z)\,\chi(z)\,\phi(x,t)\,\phi_x(x,t), \end{aligned} \tag{15}$$

$$\begin{aligned} U_3(x,z) = {} & 8C_T[\chi(z) - z]\,u_x(x,t) + 8C_T[\chi(z) - z]^2 w_{xx}(x,t) + 4C_T[\chi(z) - z]\,{w_x}^2(x,t) \\ & - 8C_T\chi(z)[\chi(z) - z]\,\phi_x(x,t) - 12C_T[\chi(z) - z]\,{u_x}^2(x,t) \\ & - 24C_T[\chi(z) - z]^2 u_x(x,t)\,w_{xx}(x,t) + 24C_T\chi(z)[\chi(z) - z]\,u_x(x,t)\,\phi_x(x,t) \\ & - 12C_T[\chi(z) - z]\,u_x(x,t)\,{w_x}^2(x,t) - 12C_T[\chi(z) - z]^3 {w_{xx}}^2(x,t) \\ & + 24C_T\chi(z)[\chi(z) - z]^2 w_{xx}(x,t)\,\phi_x(x,t) + 12C_T\chi(z)[\chi(z) - z]\,{w_x}^2(x,t)\,\phi_x(x,t) \\ & - 12C_T[\chi(z) - z]^2 {w_x}^2(x,t)\,w_{xx}(x,t) - 3C_T[\chi(z) - z]\,{w_x}^4(x,t) \\ & - 12C_T\chi(z)^2[\chi(z) - z]\,{\phi_x}^2(x,t) - C_T {\chi_z}^2(z)[\chi(z) - z]\,{w_x}^2(x,t) \\ & + 2C_T {\chi_z}^2(z)[\chi(z) - z]\,w_x(x,t)\,\phi(x,t) - C_T {\chi_z}^2(z)[\chi(z) - z]\,\phi^2(x,t), \end{aligned} \tag{16}$$

$$\begin{aligned} U_4(x,z) = {} & -2C_T {\chi_z}^2(z)\,w_x(x,t) + 2C_T {\chi_z}^2(z)\,\phi(x,t) \\ & + 2C_T {\chi_z}^2(z)\,u_x(x,t)\,w_x(x,t) - 2C_T {\chi_z}^2(z)\,u_x(x,t)\,\phi(x,t) \\ & + 2C_T {\chi_z}^2(z)[\chi(z) - z]\,w_x(x,t)\,w_{xx}(x,t) + C_T {\chi_z}^2(z)\,{w_x}^3(x,t) \\ & - 2C_T\chi(z)\,{\chi_z}^2(z)\,w_x(x,t)\,\phi_x(x,t) - C_T {\chi_z}^2(z)\,{w_x}^2(x,t)\,\phi(x,t) \\ & - 2C_T {\chi_z}^2(z)[\chi(z) - z]\,w_{xx}(x,t)\,\phi(x,t) \\ & + 2C_T\chi(z)\,{\chi_z}^2(z)\,\phi(x,t)\,\phi_x(x,t), \end{aligned} \tag{17}$$

$$
\begin{aligned}
U_5(x,z) = & -8C_T\chi(z)\,u_x(x,t) - 8C_T\chi(z)\,[\chi(z)-z]\,w_{xx}(x,t) \\
& - 4C_T\chi(z)\,{w_x}^2(x,t) + 8C_T{\chi}^2(z)\,\phi_x(x,t) + 12C_T\chi(z)\,{u_x}^2(x,t) \\
& + 24C_T\chi(z)\,[\chi(z)-z]\,u_x(x,t)\,w_{xx}(x,t) - 24C_T{\chi}^2(z)\,u_x(x,t)\,\phi_x(x,t) \\
& + 12C_T\chi(z)\,u_x(x,t)\,{w_x}^2(x,t) + 12C_T\chi(z)\,[\chi(z)-z]^2{w_{xx}}^2(x,t) \\
& - 24C_T{\chi}^2(z)\,[\chi(z)-z]\,w_{xx}(x,t)\,\phi_x(x,t) - 12C_T{\chi}^2(z)\,{w_x}^2(x,t)\,\phi_x(x,t) \\
& + 12C_T\chi(z)\,[\chi(z)-z]\,{w_x}^2(x,t)\,w_{xx}(x,t) + 3C_T\chi(z)\,{w_x}^4(x,t) \\
& + 12C_T{\chi}^3(z)\,{\phi_x}^2(x,t) + C_T\chi(z)\,{\chi_z}^2(z)\,{w_x}^2(x,t) \\
& - 2C_T\chi(z)\,{\chi_z}^2(z)\,w_x(x,t)\,\phi(x,t) + C_T\chi(z)\,{\chi_z}^2(z)\,\phi^2(x,t),
\end{aligned} \tag{18}
$$

for which, by assuming the hyperelastic beam has three layers (Fig. 1) with layers attached perfectly (with no delamination), the stiffness parameters (A_{ii}, B_{ii}, D_{ii} and E_{ii}) are defined as

$$A_{11} = \int_A C_T \mathrm{d}A = \int_{A_1} C_{T1}\mathrm{d}A_1 + \int_{A_2} C_{T2}\mathrm{d}A_2 + \int_{A_3} C_{T3}\mathrm{d}A_3, \tag{19}$$

$$B_{11} = \int_A C_T\chi(z)\,\mathrm{d}A = \int_{A_1} C_{T1}\chi(z)\,\mathrm{d}A_1 + \int_{A_2} C_{T2}\chi(z)\,\mathrm{d}A_2 + \int_{A_3} C_{T3}\chi(z)\,\mathrm{d}A_3, \tag{20}$$

$$B_{22} = \int_A C_T\,[\chi(z)-z]\,\mathrm{d}A = \int_{A_1} C_{T1}\,[\chi(z)-z]\,\mathrm{d}A_1 + \int_{A_2} C_{T2}\,[\chi(z)-z]\,\mathrm{d}A_2 + \int_{A_3} C_{T3}\,[\chi(z)-z]\,\mathrm{d}A_3, \tag{21}$$

$$D_{11} = \int_A C_T{\chi}^2(z)\mathrm{d}A = \int_{A_1} C_{T1}{\chi}^2(z)\mathrm{d}A_1 + \int_{A_2} C_{T2}{\chi}^2(z)\mathrm{d}A_2 + \int_{A_3} C_{T3}{\chi}^2(z)\mathrm{d}A_3, \tag{22}$$

$$D_{22} = \int_A C_T[\chi(z)-z]^2\mathrm{d}A = \int_{A_1} C_{T1}[\chi(z)-z]^2\mathrm{d}A_1 + \int_{A_2} C_{T2}[\chi(z)-z]^2\mathrm{d}A_2 + \int_{A_3} C_{T3}[\chi(z)-z]^2\mathrm{d}A_3, \tag{23}$$

$$D_{33} = \int_A C_T\chi(z)\,[\chi(z)-z]\mathrm{d}A = \int_{A_1} C_{T1}\chi(z)\,[\chi(z)-z]\mathrm{d}A_1 + \int_{A_2} C_{T2}\chi(z)\,[\chi(z)-z]\mathrm{d}A_2 + \int_{A_3} C_{T3}\chi(z)\,[\chi(z)-z]\mathrm{d}A_3, \tag{24}$$

$$D_{44} = \int_A C_T{\chi_z}^2(z)\mathrm{d}A = \int_{A_1} C_{T1}{\chi_z}^2(z)\mathrm{d}A_1 + \int_{A_2} C_{T2}{\chi_z}^2(z)\mathrm{d}A_2 + \int_{A_3} C_{T3}{\chi_z}^2(z)\mathrm{d}A_3, \tag{25}$$

$$E_{11} = \int_A C_T{\chi}^3(z)\,\mathrm{d}A = \int_{A_1} C_{T1}{\chi}^3(z)\,\mathrm{d}A_1 + \int_{A_2} C_{T2}{\chi}^3(z)\,\mathrm{d}A_2 + \int_{A_3} C_{T3}{\chi}^3(z)\,\mathrm{d}A_3, \tag{26}$$

$$E_{22} = \int_A C_T{\chi}^2(z)\,[\chi(z)-z]\,\mathrm{d}A = \int_{A_1} C_{T1}{\chi}^2(z)\,[\chi(z)-z]\,\mathrm{d}A_1 + \int_{A_2} C_{T2}{\chi}^2(z)\,[\chi(z)-z]\,\mathrm{d}A_2 + \int_{A_3} C_{T3}{\chi}^2(z)\,[\chi(z)-z]\,\mathrm{d}A_3, \tag{27}$$

$$E_{33} = \int_A C_T\chi(z)\,[\chi(z)-z]^2\mathrm{d}A = \int_{A_1} C_{T1}\chi(z)\,[\chi(z)-z]^2\mathrm{d}A_1$$

$$+\int_{A_2} C_{T2\chi}(z)[\chi(z)-z]^2 \mathrm{d}A_2+\int_{A_3} C_{T3\chi}(z)[\chi(z)-z]^2 \mathrm{d}A_3, \tag{28}$$

$$E_{44}=\int_A C_T[\chi(z)-z]^3 \mathrm{d}A=\int_{A_1} C_{T1}[\chi(z)-z]^3 \mathrm{d}A_1$$
$$+\int_{A_2} C_{T2}[\chi(z)-z]^3 \mathrm{d}A_2+\int_{A_3} C_{T3}[\chi(z)-z]^3 \mathrm{d}A_3, \tag{29}$$

$$E_{55}=\int_A C_T {\chi_z}^3(z)\,\mathrm{d}A=\int_{A_1} C_{T1}{\chi_z}^3(z)\,\mathrm{d}A_1+\int_{A_2} C_{T2}{\chi_z}^3(z)\,\mathrm{d}A_2+\int_{A_3} C_{T3}{\chi_z}^3(z)\,\mathrm{d}A_3, \tag{30}$$

$$E_{66}=\int_A C_T {\chi_z}^2(z)[\chi(z)-z]\,\mathrm{d}A=\int_{A_1} C_{T1}{\chi_z}^2(z)[\chi(z)-z]\,\mathrm{d}A_1$$
$$+\int_{A_2} C_{T2}{\chi_z}^2(z)[\chi(z)-z]\,\mathrm{d}A_2+\int_{A_3} C_{T3}{\chi_z}^2(z)[\chi(z)-z]\,\mathrm{d}A_3, \tag{31}$$

$$E_{77}=\int_A C_T\chi(z){\chi_z}^2(z)\,\mathrm{d}A=\int_{A_1} C_{T1}\chi(z){\chi_z}^2(z)\,\mathrm{d}A_1+\int_{A_2} C_{T2}\chi(z){\chi_z}^2(z)\,\mathrm{d}A_2$$
$$+\int_{A_3} C_{T3}\chi(z){\chi_z}^2(z)\,\mathrm{d}A_3, \tag{32}$$

which, for the case considering the Timoshenko beam model ($\chi(z)=z$), uses a shear correction factor of $\kappa=5/6$ [43]. Accordingly, by using Eqs. (19–32), the potential energy of a three-layered hyperelastic beam

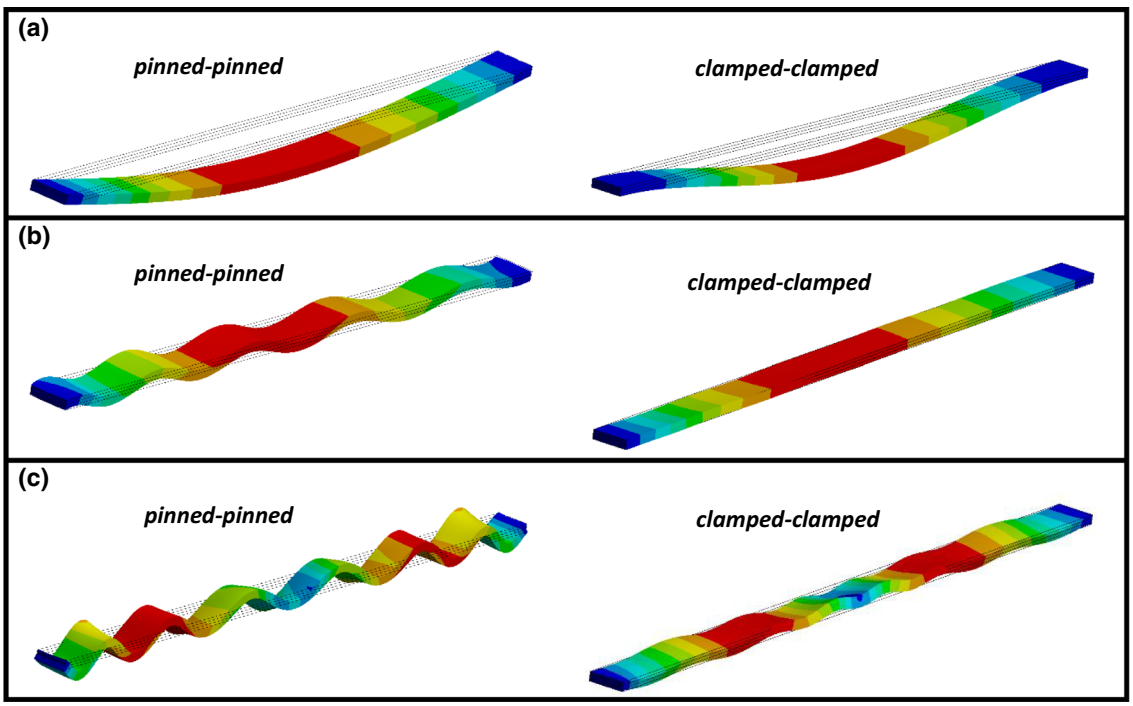

Fig. 2 Mode shapes of the first (**a**) transverse, (**b**) longitudinal and (**c**) rotation vibration modes with clamped–clamped and pinned–pinned boundary conditions

can be rewritten, which is not presented here for the sake of brevity. It should be mentioned that for having more layers in the laminated hyperelastic beam model, Eqs. (19–32) should be rewritten on the right side, based on the number of layers. The kinetic energy of the structure is written as

$$\begin{aligned}\delta KE = &\int_0^L \int_A \rho(z)\left[u_t(x,t) + (\chi(z) - z)\, w_{xt}(x,t) - \chi(z)\,\phi_t(x,t)\right]\delta u_t(x,t)\,\mathrm{d}A\mathrm{d}x \\ &+ \int_0^L \int_A \rho(z)\,(\chi(z) - z)\left[u_t(x,t) + (\chi(z) - z)\, w_{xt}(x,t) - \chi(z)\,\phi_t(x,t)\right]\delta w_{xt}(x,t)\,\mathrm{d}A\mathrm{d}x \\ &- \int_0^L \int_A \rho(z)\chi(z)\left[u_t(x,t) + (\chi(z) - z)\, w_{xt}(x,t) - \chi(z)\,\phi_t(x,t)\right]\delta\phi_t(x,t)\,\mathrm{d}A\mathrm{d}x \\ &+ \int_0^L \int_A \rho(z) w_t(x,t)\,\delta w_t(x,t)\,\mathrm{d}A\mathrm{d}x, \end{aligned} \tag{33}$$

which, by defining the moment of inertia in terms of area (I_i) for a three-layered hyperelastic thick beam, is written as

$$I_0 = \int_A \rho(z)\mathrm{d}A = \int_{A_1} \rho_1 \mathrm{d}A_1 + \int_{A_2} \rho_2 \mathrm{d}A_2 + \int_{A_3} \rho_3 \mathrm{d}A_3, \tag{34}$$

$$I_1 = \int_A \rho(z)\chi(z)\,\mathrm{d}A = \int_{A_1} \rho_1 \chi(z)\,\mathrm{d}A_1 + \int_{A_2} \rho_2 \chi(z)\,\mathrm{d}A_2 + \int_{A_3} \rho_3 \chi(z)\,\mathrm{d}A_3, \tag{35}$$

$$I_2 = \int_A \rho(z)\left[\chi(z) - z\right]\mathrm{d}A = \int_{A_1} \rho_1\left[\chi(z) - z\right]\mathrm{d}A_1 + \int_{A_2} \rho_2\left[\chi(z) - z\right]\mathrm{d}A_2 + \int_{A_3} \rho_3\left[\chi(z) - z\right]\mathrm{d}A_3, \tag{36}$$

$$I_3 = \int_A \rho(z)\,\chi^2(z)\mathrm{d}A = \int_{A_1} \rho_1 \chi^2(z)\mathrm{d}A_1 + \int_{A_2} \rho_2 \chi^2(z)\mathrm{d}A_2 + \int_{A_3} \rho_3 \chi^2(z)\mathrm{d}A_3, \tag{37}$$

$$\begin{aligned} I_4 = &\int_A \rho(z)[\chi(z) - z]^2\mathrm{d}A = \int_{A_1} \rho_1[\chi(z) - z]^2\mathrm{d}A_1 \\ &+ \int_{A_2} \rho_2[\chi(z) - z]^2\mathrm{d}A_2 + \int_{A_3} \rho_3[\chi(z) - z]^2\mathrm{d}A_3, \end{aligned} \tag{38}$$

$$\begin{aligned} I_5 = &\int_A \rho\chi(z)\left[\chi(z) - z\right]\mathrm{d}A = \int_{A_1} \rho_1\chi(z)\left[\chi(z) - z\right]\mathrm{d}A_1 \\ &+ \int_{A_2} \rho_2\chi(z)\left[\chi(z) - z\right]\mathrm{d}A_2 + \int_{A_3} \rho_3\chi(z)\left[\chi(z) - z\right]\mathrm{d}A_3, \end{aligned} \tag{39}$$

and by substituting Eqs. (34–39) into Eq. (33), one can reach the kinetic energy of layered thick hyperelastic beams, as

$$\begin{aligned}\delta KE = \int_0^L &-\left[I_0 u_{tt}(x,t) + I_2 w_{xtt}(x,t) - I_1\phi_{tt}(x,t)\right]\delta u(x,t) \\ &+\left[I_2 u_{xtt}(x,t) + I_4 w_{xxtt}(x,t) - I_5\phi_{xtt}(x,t)\right]\delta w(x,t) \\ &-I_0 w_{tt}(x,t)\,\delta w(x,t) + \left[I_1 u_{tt}(x,t) + I_5 w_{xtt}(x,t) - I_3\phi_{tt}(x,t)\right]\delta\phi(x,t)\,\mathrm{d}x. \end{aligned} \tag{40}$$

Moreover, the beam is assumed to be lying on a nonlinear elastic foundation (Fig. 1) and externally actuated by a periodic load, which gives the external work on the beam as

$$\begin{aligned}\delta U_F &= \int_0^L \left(F_{linear}\left(x,t\right)+F_{nonlinear}\left(x,t\right)+F_{shear}\left(x,t\right)\right)\delta w\mathrm{d}x+\int_0^L F\cos\left(\omega t\right)\delta w\mathrm{d}x\\ &= \int_0^L \left[-K_L w\left(x,t\right)-K_{NL}w^3\left(x,t\right)+K_S w_{xx}\left(x,t\right)+F\cos\left(\omega t\right)\right]\delta w, \end{aligned} \tag{41}$$

where K_L, K_{NL} and K_S are the linear, nonlinear and shear coefficients of the foundation, respectively, and F is the external force acting periodically with a frequency of ω. Using Hamilton's principle, the coupled longitudinal, transverse and rotation equations of motion are obtained as

$$\begin{aligned}&I_0 u_{tt}\left(x,t\right)+I_2 w_{xtt}\left(x,t\right)-I_1\phi_{tt}\left(x,t\right)-8A_{11}u_{xx}\left(x,t\right)-8B_{22}w_{xxx}\left(x,t\right)+8B_{11}\phi_{xx}\left(x,t\right)\\ &+12A_{11}\frac{\partial}{\partial x}\left[{u_x}^2\left(x,t\right)\right]+24B_{22}\frac{\partial}{\partial x}\left[u_x\left(x,t\right)w_{xx}\left(x,t\right)\right]-24B_{11}\frac{\partial}{\partial x}\left[u_x\left(x,t\right)\phi_x\left(x,t\right)\right]\\ &-\left(4A_{11}-D_{44}\right)\frac{\partial}{\partial x}\left[{w_x}^2\left(x,t\right)\right]+12D_{22}\frac{\partial}{\partial x}\left[{w_{xx}}^2\left(x,t\right)\right]-2D_{44}\frac{\partial}{\partial x}\left[w_x\left(x,t\right)\phi\left(x,t\right)\right]\\ &-24D_{33}\frac{\partial}{\partial x}\left[w_{xx}\left(x,t\right)\phi_x\left(x,t\right)\right]+D_{44}\frac{\partial}{\partial x}\left[\phi^2\left(x,t\right)\right]+12D_{11}\frac{\partial}{\partial x}\left[{\phi_x}^2\left(x,t\right)\right]\\ &+12A_{11}\frac{\partial}{\partial x}\left[u_x\left(x,t\right){w_x}^2\left(x,t\right)\right]+12B_{22}\frac{\partial}{\partial x}\left[{w_x}^2\left(x,t\right)w_{xx}\left(x,t\right)\right]\\ &-12B_{11}\frac{\partial}{\partial x}\left[{w_x}^2\left(x,t\right)\phi_x\left(x,t\right)\right]+3A_{11}\frac{\partial}{\partial x}\left[{w_x}^4\left(x,t\right)\right]=0, \end{aligned} \tag{42}$$

$$\begin{aligned}&-I_2 u_{xtt}\left(x,t\right)+I_0 w_{tt}\left(x,t\right)-I_4 w_{xxtt}\left(x,t\right)+I_5\phi_{xtt}\left(x,t\right)-8B_{22}u_{xxx}\left(x,t\right)-2D_{44}w_{xx}\left(x,t\right)\\ &-8D_{22}w_{xxxx}\left(x,t\right)+K_L w\left(x,t\right)-K_S w_{xx}\left(x,t\right)+2D_{44}\phi_x\left(x,t\right)+8D_{33}\phi_{xxx}\left(x,t\right)\\ &+12B_{22}\frac{\partial^2}{\partial x^2}\left[{u_x}^2\left(x,t\right)\right]+24D_{22}\frac{\partial^2}{\partial x^2}\left[u_x\left(x,t\right)w_{xx}\left(x,t\right)\right]\\ &-\left(8A_{11}-2D_{44}\right)\frac{\partial}{\partial x}\left[u_x\left(x,t\right)w_x\left(x,t\right)\right]-24D_{33}\frac{\partial^2}{\partial x^2}\left[u_x\left(x,t\right)\phi_x\left(x,t\right)\right]\\ &-2D_{44}\frac{\partial}{\partial x}\left[u_x\left(x,t\right)\phi\left(x,t\right)\right]-\left(4B_{22}-E_{66}\right)\frac{\partial^2}{\partial x^2}\left[{w_x}^2\left(x,t\right)\right]\\ &-\left(8B_{22}-2E_{66}\right)\frac{\partial}{\partial x}\left[w_x\left(x,t\right)w_{xx}\left(x,t\right)\right]+12E_{44}\frac{\partial^2}{\partial x^2}\left[{w_{xx}}^2\left(x,t\right)\right]\\ &-2E_{66}\frac{\partial^2}{\partial x^2}\left[w_x\left(x,t\right)\phi\left(x,t\right)\right]+\left(8B_{11}-2E_{77}\right)\frac{\partial}{\partial x}\left[w_x\left(x,t\right)\phi_x\left(x,t\right)\right]\\ &-2E_{66}\frac{\partial}{\partial x}\left[w_{xx}\left(x,t\right)\phi\left(x,t\right)\right]-24E_{33}\frac{\partial^2}{\partial x^2}\left[w_{xx}\left(x,t\right)\phi_x\left(x,t\right)\right]\\ &+E_{66}\frac{\partial^2}{\partial x^2}\left[\phi^2\left(x,t\right)\right]+2E_{77}\frac{\partial}{\partial x}\left[\phi\left(x,t\right)\phi_x\left(x,t\right)\right]+12E_{22}\frac{\partial^2}{\partial x^2}\left[{\phi_x}^2\left(x,t\right)\right]\\ &+12A_{11}\frac{\partial}{\partial x}\left[{u_x}^2\left(x,t\right)w_x\left(x,t\right)\right]+12B_{22}\frac{\partial^2}{\partial x^2}\left[u_x\left(x,t\right){w_x}^2\left(x,t\right)\right]\\ &+24B_{22}\frac{\partial}{\partial x}\left[u_x\left(x,t\right)w_x\left(x,t\right)w_{xx}\left(x,t\right)\right]-24B_{11}\frac{\partial}{\partial x}\left[u_x\left(x,t\right)w_x\left(x,t\right)\phi_x\left(x,t\right)\right]\\ &-\left(4A_{11}-2D_{44}\right)\frac{\partial}{\partial x}\left[{w_x}^3\left(x,t\right)\right]+K_{NL}w^3\left(x,t\right)+12D_{22}\frac{\partial}{\partial x}\left[w_x\left(x,t\right){w_{xx}}^2\left(x,t\right)\right]\\ &+12D_{22}\frac{\partial^2}{\partial x^2}\left[{w_x}^2\left(x,t\right)w_{xx}\left(x,t\right)\right]-12D_{33}\frac{\partial^2}{\partial x^2}\left[{w_x}^2\left(x,t\right)\phi_x\left(x,t\right)\right]\\ &-3D_{44}\frac{\partial}{\partial x}\left[{w_x}^2\left(x,t\right)\phi\left(x,t\right)\right]-24D_{33}\frac{\partial}{\partial x}\left[w_x\left(x,t\right)w_{xx}\left(x,t\right)\phi_x\left(x,t\right)\right] \end{aligned}$$

$$+ D_{44}\frac{\partial}{\partial x}\left[w_x\left(x,t\right)\phi^2\left(x,t\right)\right] + 12D_{11}\frac{\partial}{\partial x}\left[w_x\left(x,t\right)\phi_x{}^2\left(x,t\right)\right]$$
$$+ 12A_{11}\frac{\partial}{\partial x}\left[u_x\left(x,t\right)w_x{}^3\left(x,t\right)\right] + 3B_{22}\frac{\partial^2}{\partial x^2}\left[w_x{}^4\left(x,t\right)\right] + 12B_{22}\frac{\partial}{\partial x}\left[w_x{}^3\left(x,t\right)w_{xx}\left(x,t\right)\right]$$
$$- 12B_{11}\frac{\partial}{\partial x}\left[w_x{}^3\left(x,t\right)\phi_x\left(x,t\right)\right] + 3A_{11}\frac{\partial}{\partial x}\left[w_x{}^5\left(x,t\right)\right] = F\cos\left(\omega t\right), \tag{43}$$

$$-I_1u_{tt}\left(x,t\right) - I_5w_{xtt}\left(x,t\right) + I_3\phi_{tt}\left(x,t\right) + 8B_{11}u_{xx}\left(x,t\right) - 2D_{44}w_x\left(x,t\right) + 8D_{33}w_{xxx}\left(x,t\right)$$
$$- 8D_{11}\phi_{xx}\left(x,t\right) + 2D_{44}\phi\left(x,t\right) - 12B_{11}\frac{\partial}{\partial x}\left[u_x{}^2\left(x,t\right)\right] - 24D_{33}\frac{\partial}{\partial x}\left[u_x\left(x,t\right)w_{xx}\left(x,t\right)\right]$$
$$+ 2D_{44}u_x\left(x,t\right)w_x\left(x,t\right) + 24D_{11}\frac{\partial}{\partial x}\left[u_x\left(x,t\right)\phi_x\left(x,t\right)\right] - 2D_{44}u_x\left(x,t\right)\phi\left(x,t\right)$$
$$+ \left(4B_{11} - E_{77}\right)\frac{\partial}{\partial x}\left[w_x{}^2\left(x,t\right)\right] - 12E_{33}\frac{\partial}{\partial x}\left[w_{xx}{}^2\left(x,t\right)\right] + 2E_{66}w_x\left(x,t\right)w_{xx}\left(x,t\right)$$
$$+ 2E_{77}\frac{\partial}{\partial x}\left[w_x\left(x,t\right)\phi\left(x,t\right)\right] + 24E_{22}\frac{\partial}{\partial x}\left[w_{xx}\left(x,t\right)\phi_x\left(x,t\right)\right] - 2E_{77}w_x\left(x,t\right)\phi_x\left(x,t\right)$$
$$- 2E_{66}w_{xx}\left(x,t\right)\phi\left(x,t\right) - 12E_{11}\frac{\partial}{\partial x}\left[\phi_x{}^2\left(x,t\right)\right] - E_{77}\frac{\partial}{\partial x}\left[\phi^2\left(x,t\right)\right] + 2E_{77}\phi\left(x,t\right)\phi_x\left(x,t\right)$$
$$- 12B_{11}\frac{\partial}{\partial x}\left[u_x\left(x,t\right)w_x{}^2\left(x,t\right)\right] - 12D_{33}\frac{\partial}{\partial x}\left[w_x{}^2\left(x,t\right)w_{xx}\left(x,t\right)\right] + D_{44}w_x{}^3\left(x,t\right)$$
$$+ 12D_{11}\frac{\partial}{\partial x}\left[w_x{}^2\left(x,t\right)\phi_x\left(x,t\right)\right] - D_{44}w_x{}^2\left(x,t\right)\phi\left(x,t\right) - 3B_{11}\frac{\partial}{\partial x}\left[w_x{}^4\left(x,t\right)\right] = 0. \tag{44}$$

It can therefore be seen that the equations of motion are highly nonlinear and coupled, which emphasises the importance of having the axial motion while analysing the mechanical behaviour of the structure. The linear coupling sources between the axial and transverse motions are the stiffness terms B_{11} and B_{22} and inertia terms I_1 and I_2, for which, for a single-layer hyperelastic beam, due to the homogeneity in the thickness direction, these terms will be equal to zero and the linear coupling terms vanish. In the next section, the equations of motion are nondimensionalised, discretised and solved.

3 Solution procedure

For the first step of solving the equations of motion, the new nondimensional parameters are defined as

$$\gamma^* = \frac{x}{L}, \beta^* = \frac{w}{h}, \alpha^* = \frac{u}{h}, \phi^* = \phi, A_{11}{}^* = \frac{A_{11}}{A_{110}}, B_{11}{}^* = \frac{B_{11}}{A_{110}h}, B_{22}{}^* = \frac{B_{22}}{A_{110}h}, D_{44}{}^* = \frac{D_{11}}{A_{110}},$$
$$D_{11}{}^* = \frac{D_{11}}{A_{110}h^2}, D_{22}{}^* = \frac{D_{11}}{A_{110}h^2}, D_{33}{}^* = \frac{D_{11}}{A_{110}h^2}, E_{11}{}^* = \frac{E_{11}}{A_{110}h^3}, E_{22}{}^* = \frac{E_{22}}{A_{110}h^3},$$
$$E_{33}{}^* = \frac{E_{33}}{A_{110}h^3}, E_{44}{}^* = \frac{E_{44}}{A_{110}h^3}, E_{55}{}^* = \frac{E_{55}}{A_{110}}, E_{66}{}^* = \frac{E_{66}}{A_{110}h}, E_{77}{}^* = \frac{E_{77}}{A_{110}h},$$
$$I_0{}^* = \frac{I_0}{I_{00}}, I_1{}^* = \frac{I_1}{I_{00}h}, I_2{}^* = \frac{I_2}{I_{00}h}, I_3{}^* = \frac{I_3}{I_{00}h^2}, I_4{}^* = \frac{I_4}{I_{00}h^2}, I_5{}^* = \frac{I_5}{I_{00}h^2},$$
$$\eta = \frac{h}{L}, \Omega = \omega\sqrt{\frac{I_{00}L^3}{A_{110}h}}, t^* = t\sqrt{\frac{A_{110}h}{I_{00}L^3}},$$
$$F^* = F\frac{L^2}{A_{11}h}, K_L{}^* = K_L\frac{L^2}{A_{11}}, K_{NL}{}^* = K_{NL}\frac{h^2L^2}{A_{11}}, K_S{}^* = K_S\frac{1}{A_{11}}, \tag{45}$$

and by using these terms, the equations of motion are nondimensionalised as

$$I_0\eta\alpha_{tt}\left(\gamma,t\right) + I_2\eta^2\beta_{\gamma tt}\left(\gamma,t\right) - I_1\eta\phi_{tt}\left(\gamma,t\right) - 8A_{11}\alpha_{\gamma\gamma}\left(\gamma,t\right) - 8B_{22}\eta\beta_{\gamma\gamma\gamma}\left(\gamma,t\right) + 8B_{11}\phi_{\gamma\gamma}\left(\gamma,t\right)$$

$$
\begin{aligned}
&+12A_{11}\eta\frac{\partial}{\partial\gamma}\left[{\alpha_\gamma}^2(\gamma,t)\right]+24B_{22}\eta^2\frac{\partial}{\partial\gamma}\left[\alpha_\gamma(\gamma,t)\,\beta_{\gamma\gamma}(\gamma,t)\right]-24B_{11}\eta\frac{\partial}{\partial\gamma}\left[\alpha_\gamma(\gamma,t)\,\phi_\gamma(\gamma,t)\right]\\
&-\eta(4A_{11}-D_{44})\frac{\partial}{\partial\gamma}\left[{\beta_\gamma}^2(\gamma,t)\right]+12D_{22}\eta^3\frac{\partial}{\partial\gamma}\left[{\beta_{\gamma\gamma}}^2(\gamma,t)\right]-2D_{44}\frac{\partial}{\partial\gamma}\left[\beta_\gamma(\gamma,t)\,\phi(\gamma,t)\right]\\
&-24D_{33}\eta^2\frac{\partial}{\partial\gamma}\left[\beta_{\gamma\gamma}(\gamma,t)\,\phi_\gamma(\gamma,t)\right]+D_{44}\frac{1}{\eta}\frac{\partial}{\partial\gamma}\left[\phi^2(\gamma,t)\right]+12D_{11}\eta\frac{\partial}{\partial\gamma}\left[{\phi_\gamma}^2(\gamma,t)\right]\\
&+12A_{11}\eta^2\frac{\partial}{\partial\gamma}\left[\alpha_\gamma(\gamma,t)\,{\beta_\gamma}^2(\gamma,t)\right]+12B_{22}\eta^3\frac{\partial}{\partial\gamma}\left[{\beta_\gamma}^2(\gamma,t)\,\beta_{\gamma\gamma}(\gamma,t)\right]\\
&-12B_{11}\eta^2\frac{\partial}{\partial\gamma}\left[{\beta_\gamma}^2(\gamma,t)\,\phi_\gamma(\gamma,t)\right]+3A_{11}\eta^3\frac{\partial}{\partial\gamma}\left[{\beta_\gamma}^4(\gamma,t)\right]=0,
\end{aligned}
\tag{46}
$$

$$
\begin{aligned}
&-I_2\eta^2\alpha_{\gamma tt}(\gamma,t)+I_0\eta\beta_{tt}(\gamma,t)-I_4\eta^3\beta_{\gamma\gamma tt}(\gamma,t)+I_5\eta^2\phi_{\gamma tt}(\gamma,t)-8B_{22}\eta\alpha_{\gamma\gamma\gamma}(\gamma,t)\\
&-2D_{44}\beta_{\gamma\gamma}(\gamma,t)-8D_{22}\eta^2\beta_{\gamma\gamma\gamma\gamma}(\gamma,t)+K_L\beta(\gamma,t)-K_S\beta_{\gamma\gamma}(\gamma,t)+2D_{44}\frac{1}{\eta}\phi_\gamma(\gamma,t)\\
&+8D_{33}\eta\phi_{\gamma\gamma\gamma}(\gamma,t)+12B_{22}\eta^2\frac{\partial^2}{\partial\gamma^2}\left[{\alpha_\gamma}^2(\gamma,t)\right]+24D_{22}\eta^3\frac{\partial^2}{\partial\gamma^2}\left[\alpha_\gamma(\gamma,t)\,\beta_{\gamma\gamma}(\gamma,t)\right]\\
&-\eta(8A_{11}-2D_{44})\frac{\partial}{\partial\gamma}\left[\alpha_\gamma(\gamma,t)\,\beta_\gamma(\gamma,t)\right]-24D_{33}\eta^2\frac{\partial^2}{\partial\gamma^2}\left[\alpha_\gamma(\gamma,t)\,\phi_\gamma(\gamma,t)\right]\\
&-2D_{44}\frac{\partial}{\partial\gamma}\left[\alpha_\gamma(\gamma,t)\,\phi(\gamma,t)\right]-\eta^2(4B_{22}-E_{66})\frac{\partial^2}{\partial\gamma^2}\left[{\beta_\gamma}^2(\gamma,t)\right]\\
&-\eta^2(8B_{22}-2E_{66})\frac{\partial}{\partial\gamma}\left[\beta_\gamma(\gamma,t)\,\beta_{\gamma\gamma}(\gamma,t)\right]+12E_{44}\eta^4\frac{\partial^2}{\partial\gamma^2}\left[{\beta_{\gamma\gamma}}^2(\gamma,t)\right]\\
&-2E_{66}\eta\frac{\partial^2}{\partial\gamma^2}\left[\beta_\gamma(\gamma,t)\,\phi(\gamma,t)\right]+\eta(8B_{11}-2E_{77})\frac{\partial}{\partial\gamma}\left[\beta_\gamma(\gamma,t)\,\phi_\gamma(\gamma,t)\right]\\
&-2E_{66}\eta\frac{\partial}{\partial\gamma}\left[\beta_{\gamma\gamma}(\gamma,t)\,\phi(\gamma,t)\right]-24E_{33}\eta^3\frac{\partial^2}{\partial\gamma^2}\left[\beta_{\gamma\gamma}(\gamma,t)\,\phi_\gamma(\gamma,t)\right]\\
&+E_{66}\frac{\partial^2}{\partial\gamma^2}\left[\phi^2(\gamma,t)\right]+2E_{77}\frac{\partial}{\partial\gamma}\left[\phi(\gamma,t)\,\phi_\gamma(\gamma,t)\right]+12E_{22}\eta^2\frac{\partial^2}{\partial\gamma^2}\left[{\phi_\gamma}^2(\gamma,t)\right]\\
&+12A_{11}\eta^2\frac{\partial}{\partial\gamma}\left[{\alpha_\gamma}^2(\gamma,t)\,\beta_\gamma(\gamma,t)\right]+12B_{22}\eta^3\frac{\partial^2}{\partial\gamma^2}\left[\alpha_\gamma(\gamma,t)\,{\beta_\gamma}^2(\gamma,t)\right]\\
&+24B_{22}\eta^3\frac{\partial}{\partial\gamma}\left[\alpha_\gamma(\gamma,t)\,\beta_\gamma(\gamma,t)\,\beta_{\gamma\gamma}(\gamma,t)\right]-24B_{11}\eta^2\frac{\partial}{\partial\gamma}\left[\alpha_\gamma(\gamma,t)\,\beta_\gamma(\gamma,t)\,\phi_\gamma(\gamma,t)\right]\\
&-\eta^2(4A_{11}-2D_{44})\frac{\partial}{\partial\gamma}\left[{\beta_\gamma}^3(\gamma,t)\right]+K_{NL}\beta^3(\gamma,t)+12D_{22}\eta^4\frac{\partial}{\partial\gamma}\left[\beta_\gamma(\gamma,t)\,{\beta_{\gamma\gamma}}^2(\gamma,t)\right]\\
&+12D_{22}\eta^4\frac{\partial^2}{\partial\gamma^2}\left[{\beta_\gamma}^2(\gamma,t)\,\beta_{\gamma\gamma}(\gamma,t)\right]-12D_{33}\eta^3\frac{\partial^2}{\partial\gamma^2}\left[{\beta_\gamma}^2(\gamma,t)\,\phi_\gamma(\gamma,t)\right]\\
&-3D_{44}\eta\frac{\partial}{\partial\gamma}\left[{\beta_\gamma}^2(\gamma,t)\,\phi(\gamma,t)\right]-24D_{33}\eta^3\frac{\partial}{\partial\gamma}\left[\beta_\gamma(\gamma,t)\,\beta_{\gamma\gamma}(\gamma,t)\,\phi_\gamma(\gamma,t)\right]\\
&+D_{44}\frac{\partial}{\partial\gamma}\left[\beta_\gamma(\gamma,t)\,\phi^2(\gamma,t)\right]+12D_{11}\eta^2\frac{\partial}{\partial\gamma}\left[\beta_\gamma(\gamma,t)\,{\phi_\gamma}^2(\gamma,t)\right]\\
&+12A_{11}\eta^3\frac{\partial}{\partial\gamma}\left[\alpha_\gamma(\gamma,t)\,{\beta_\gamma}^3(\gamma,t)\right]+3B_{22}\eta^4\frac{\partial^2}{\partial\gamma^2}\left[{\beta_\gamma}^4(\gamma,t)\right]\\
&+12B_{22}\eta^4\frac{\partial}{\partial\gamma}\left[{\beta_\gamma}^3(\gamma,t)\,\beta_{\gamma\gamma}(\gamma,t)\right]-12B_{11}\eta^3\frac{\partial}{\partial\gamma}\left[{\beta_\gamma}^3(\gamma,t)\,\beta_\gamma(\gamma,t)\right]\\
&+3A_{11}\eta^4\frac{\partial}{\partial\gamma}\left[{\beta_\gamma}^5(\gamma,t)\right]=F\cos(\Omega t),
\end{aligned}
\tag{47}
$$

$$
\begin{aligned}
&-I_1\eta\alpha_{tt}(\gamma,t)-I_5\eta^2\beta_{\gamma tt}(\gamma,t)+I_3\eta\phi_{tt}(\gamma,t)+8B_{11}\alpha_{\gamma\gamma}(\gamma,t)-2D_{44}\frac{1}{\eta}\beta_\gamma(\gamma,t)+8D_{33}\eta\beta_{\gamma\gamma\gamma}(\gamma,t)\\
&-8D_{11}\phi_{\gamma\gamma}(\gamma,t)+2D_{44}\frac{1}{\eta^2}\phi(\gamma,t)-12B_{11}\eta\frac{\partial}{\partial\gamma}\left[{\alpha_\gamma}^2(\gamma,t)\right]-24D_{33}\eta^2\frac{\partial}{\partial\gamma}\left[\alpha_\gamma(\gamma,t)\beta_{\gamma\gamma}(\gamma,t)\right]\\
&+2D_{44}\alpha_\gamma(\gamma,t)\beta_\gamma(\gamma,t)+24D_{11}\eta\frac{\partial}{\partial\gamma}\left[\alpha_\gamma(\gamma,t)\phi_\gamma(\gamma,t)\right]-2D_{44}\frac{1}{\eta}\alpha_\gamma\phi(x,t)\\
&+(4B_{11}-E_{77})\eta\frac{\partial}{\partial\gamma}\left[{\beta_\gamma}^2(\gamma,t)\right]-12E_{33}\eta^3\frac{\partial}{\partial\gamma}\left[{\beta_{\gamma\gamma}}^2(\gamma,t)\right]+2E_{66}\eta\beta_\gamma(\gamma,t)\beta_{\gamma\gamma}(\gamma,t)\\
&+2E_{77}\frac{\partial}{\partial\gamma}\left[\beta_\gamma(\gamma,t)\phi(\gamma,t)\right]+24E_{22}\eta^2\frac{\partial}{\partial\gamma}\left[\beta_{\gamma\gamma}(\gamma,t)\phi_\gamma(\gamma,t)\right]-2E_{77}\beta_\gamma(\gamma,t)\phi_\gamma(\gamma,t)\\
&-2E_{66}\beta_{\gamma\gamma}(\gamma,t)\phi(\gamma,t)-12E_{11}\eta\frac{\partial}{\partial\gamma}\left[{\phi_\gamma}^2(\gamma,t)\right]-E_{77}\frac{1}{\eta}\frac{\partial}{\partial\gamma}\left[\phi^2(\gamma,t)\right]+2E_{77}\frac{1}{\eta}\phi(\gamma,t)\phi_\gamma(\gamma,t)\\
&-12B_{11}\eta^2\frac{\partial}{\partial\gamma}\left[\alpha_\gamma(\gamma,t){\beta_\gamma}^2(\gamma,t)\right]-12D_{33}\eta^3\frac{\partial}{\partial\gamma}\left[{\beta_\gamma}^2(\gamma,t)\beta_{\gamma\gamma}(\gamma,t)\right]+D_{44}\eta{\beta_\gamma}^3(\gamma,t)\\
&+12D_{11}\eta^2\frac{\partial}{\partial\gamma}\left[{\beta_\gamma}^2(\gamma,t)\phi_\gamma(\gamma,t)\right]-D_{44}{\beta_\gamma}^2(\gamma,t)\phi(\gamma,t)-3B_{11}\eta^3\frac{\partial}{\partial x}\left[{\beta_\gamma}^4(\gamma,t)\right]=0.
\end{aligned}
\tag{48}
$$

For the sake of brevity and ease notation, the superscript * is neglected in the formulation. Using the Galerkin scheme, each motion component can be written in a series expansion of orthogonal spatial functions as

$$
\begin{Bmatrix}\alpha\\ \phi\\ \beta\end{Bmatrix}=\sum_{n=1}^{N}\begin{Bmatrix}U_n(\gamma)r_n(t)\\ \Phi_n(\gamma)p_n(t)\\ W_n(\gamma)q_n(t)\end{Bmatrix},
\tag{49}
$$

where U_n, Φ_n, W_n are the set of trial functions that should satisfy the boundary conditions of longitudinal, rotation and transverse motions at the middle of the thickness. (Studies on layered structures based on various thickness assumptions can be found in Refs. [44–50].) For pinned–pinned and fixed–fixed boundary conditions, these trial functions are written as

$$
U_p(\gamma)=\sin\left(\mu_p\gamma\right),
\tag{50}
$$

$$
\begin{cases}Fixed-Fixed\rightarrow W_p(\gamma)=-\cos\left(\mu_p\gamma\right)+\cosh\left(\mu_p\gamma\right)-\psi\left(\mu_p\right)\left[-\sin\left(\mu_p\gamma\right)+\sinh\left(\mu_p\gamma\right)\right],\\ Pinned-Pinned\rightarrow W_p(\gamma)=\sin\left(\mu_p\gamma\right),\end{cases}
\tag{51}
$$

$$
\Phi_p(\gamma)=\left(\frac{1}{\mu_p}\right)\left(\frac{\partial W_p(\gamma)}{\partial x}\right),
\tag{52}
$$

where

$$
\psi\left(\mu_p\right)=\frac{-\cos\left(\mu_p\right)+\cosh\left(\mu_p\right)}{-\sin\left(\mu_p\right)+\sinh\left(\mu_p\right)},
\tag{53}
$$

and the equations of motion are rewritten as

$$
\begin{aligned}
&\begin{bmatrix}\boldsymbol{M}_{11}&\boldsymbol{M}_{12}&\boldsymbol{M}_{13}\\ \boldsymbol{M}_{21}&\boldsymbol{M}_{22}&\boldsymbol{M}_{23}\\ \boldsymbol{M}_{31}&\boldsymbol{M}_{32}&\boldsymbol{M}_{33}\end{bmatrix}\begin{Bmatrix}\ddot{r}_n\\ \ddot{p}_n\\ \ddot{q}_n\end{Bmatrix}+\begin{bmatrix}\xi&0&0\\ 0&\xi&0\\ 0&0&\xi\end{bmatrix}\begin{Bmatrix}\dot{r}_n\\ \dot{p}_n\\ \dot{q}_n\end{Bmatrix}\\
&+\begin{bmatrix}\boldsymbol{KL}_{11}&\boldsymbol{KL}_{12}&\boldsymbol{KL}_{13}\\ \boldsymbol{KL}_{21}&\boldsymbol{KL}_{22}&\boldsymbol{KL}_{23}\\ \boldsymbol{KL}_{31}&\boldsymbol{KL}_{32}&\boldsymbol{KL}_{33}\end{bmatrix}\begin{Bmatrix}r_n\\ p_n\\ q_n\end{Bmatrix}=\begin{Bmatrix}0\\ 0\\ F_n^{external}\end{Bmatrix}+\begin{Bmatrix}\boldsymbol{KN1}_n^{system}\\ \boldsymbol{KN2}_n^{system}\\ \boldsymbol{KN3}_n^{system}\end{Bmatrix},
\end{aligned}
\tag{54}
$$

where $\boldsymbol{M}_{ij}$ are the mass tensors of the discretised equations and the components are defined as

$$
M_{11}(l,i):\eta I_0\int_0^1 U_l(\gamma)U_i(\gamma)\,\mathrm{d}\gamma,
\tag{55}
$$

$$M_{12}(l,i) : \eta^2 I_2 \int_0^1 U_l(\gamma) W_i'(\gamma)\,\mathrm{d}\gamma, \tag{56}$$

$$M_{13}(l,i) : -\eta I_1 \int_0^1 U_l(\gamma) \Phi_i(\gamma)\,\mathrm{d}\gamma, \tag{57}$$

$$M_{21} : -\eta^2 I_2 \int_0^1 W_l(\gamma) U_i'(\gamma)\,\mathrm{d}\gamma, \tag{58}$$

$$M_{22}(l,i) : \eta I_0 \int_0^1 W_l(\gamma) W_i(\gamma)\,\mathrm{d}\gamma - \eta^3 I_4 \int_0^1 W_l(\gamma) W_i''(\gamma)\,\mathrm{d}\gamma, \tag{59}$$

$$M_{23}(l,i) : \eta^2 I_5 \int_0^1 W_l(\gamma) \Phi_i'(\gamma)\,\mathrm{d}\gamma, \tag{60}$$

$$M_{31} : -\eta I_1 \int_0^1 \Phi_l(\gamma) U_i(\gamma)\,\mathrm{d}\gamma, \tag{61}$$

$$M_{32}(l,i) : -\eta^2 I_5 \int_0^1 \Phi_l(\gamma) W_i'(\gamma)\,\mathrm{d}\gamma, \tag{62}$$

$$M_{33}(l,i) : \eta I_3 \int_0^1 \Phi_l(\gamma) \Phi_i(\gamma)\,\mathrm{d}\gamma, \tag{63}$$

and $\boldsymbol{KL}_{ij}$ are the linear stiffness tensors, defined as

$$KL_{11}(l,i) : -8A_{11} \int_0^1 U_l(\gamma) U_i''(\gamma)\,\mathrm{d}\gamma, \tag{64}$$

$$KL_{12}(l,i) : -8\eta B_{22} \int_0^1 U_l(\gamma) W_i'''(\gamma)\,\mathrm{d}\gamma, \tag{65}$$

$$KL_{13}(l,i) : 8B_{11} \int_0^1 U_l(\gamma) \Phi_i''(\gamma)\,\mathrm{d}\gamma, \tag{66}$$

$$KL_{21}(l,i) : -8\eta B_{22} \int_0^1 W_l(\gamma) U_i'''(\gamma)\,\mathrm{d}\gamma, \tag{67}$$

$$\begin{aligned} KL_{22}(l,i) : &- \int_0^1 W_l(\gamma) \frac{\mathrm{d}}{\mathrm{d}\gamma} \left[2D_{44} W'_i(\gamma)\right] \mathrm{d}\gamma - 8\eta^2 D_{22} \int_0^1 W_l(\gamma) W_i^{(4)}(\gamma)\,\mathrm{d}\gamma \\ &+ K_L \int_0^1 W_l(\gamma) W_i(\gamma)\,\mathrm{d}\gamma - K_S \int_0^1 W_l(\gamma) W''_i(\gamma)\,\mathrm{d}\gamma, \end{aligned} \tag{68}$$

$$KL_{23}(l,i): 2\frac{1}{\eta}D_{44}\int_0^1 W_l(\gamma)\Phi_i'(\gamma)\,\mathrm{d}\gamma + 8\eta D_{33}\int_0^1 W_l(\gamma)\Phi_i'''(\gamma)\,\mathrm{d}\gamma, \tag{69}$$

$$KL_{31}(l,i): 8B_{11}\int_0^1 \Phi_l(\gamma)U_i''(\gamma)\,\mathrm{d}\gamma, \tag{70}$$

$$KL_{32}(l,i): -2\frac{1}{\eta}D_{44}\int_0^1 \Phi_l(\gamma)W_i'(\gamma)\,\mathrm{d}\gamma + 8\eta D_{33}\int_0^1 \Phi_l(\gamma)W_i'''(\gamma)\,\mathrm{d}\gamma, \tag{71}$$

$$KL_{33}(l,i): -8D_{11}\int_0^1 \Phi_l(\gamma)\Phi_i''(\gamma)\,\mathrm{d}\gamma + 2\frac{1}{\eta^2}D_{44}\int_0^1 \Phi_l(\gamma)\Phi_i(\gamma)\,\mathrm{d}\gamma. \tag{72}$$

$KN1$, $KN2$ and $KN3$ are the nonlinear stiffness terms in the coupled equation where

$$\begin{aligned}
\boldsymbol{KN}1_n^{system} &= \boldsymbol{KN}_{11}r^2(t) + \boldsymbol{KN}_{12}r(t)\,p(t) + \boldsymbol{KN}_{13}r(t)\,q(t)\\
&+ \boldsymbol{KN}_{14}p^2(t) + \boldsymbol{KN}_{15}p(t)\,q(t) + \boldsymbol{KN}_{16}q^2(t)\\
&+ \boldsymbol{KN}_{17}r(t)\,p^2(t) + \boldsymbol{KN}_{18}p^3(t) + \boldsymbol{KN}_{19}p^2(t)\,q(t)\\
&+ \boldsymbol{KN}_{110}p^4(t),
\end{aligned} \tag{73}$$

$$\begin{aligned}
\boldsymbol{KN}2_n^{system} &= \boldsymbol{KN}_{21}r^2(t) + \boldsymbol{KN}_{22}r(t)\,p(t) + \boldsymbol{KN}_{23}r(t)\,q(t)\\
&+ \boldsymbol{KN}_{24}p^2(t) + \boldsymbol{KN}_{25}p(t)\,q(t) + \boldsymbol{KN}_{26}q^2(t)\\
&+ \boldsymbol{KN}_{27}r^2(t)\,p(t) + \boldsymbol{KN}_{28}r(t)\,p^2(t)\\
&+ \boldsymbol{KN}_{29}r(t)\,p(t)\,q(t) + \boldsymbol{KN}_{210}p^3(t)\\
&+ \boldsymbol{KN}_{211}p^2(t)\,q(t) + \boldsymbol{KN}_{212}p(t)\,q^2(t)\\
&+ \boldsymbol{KN}_{213}r(t)\,p^3(t) + \boldsymbol{KN}_{214}p^4(t) + \boldsymbol{KN}_{215}p^3(t)\,q(t) + \boldsymbol{KN}_{216}p^5(t),
\end{aligned} \tag{74}$$

$$\begin{aligned}
\boldsymbol{KN}3_n^{system} &= \boldsymbol{KN}_{31}r^2(t) + \boldsymbol{KN}_{32}r(t)\,p(t) + \boldsymbol{KN}_{33}r(t)\,q(t) + \boldsymbol{KN}_{34}p^2(t)\\
&+ \boldsymbol{KN}_{35}p(t)\,q(t) + \boldsymbol{KN}_{36}q^2(t) + \boldsymbol{KN}_{37}r(t)\,p^2(t) + \boldsymbol{KN}_{38}p^3(t)\\
&+ \boldsymbol{KN}_{39}p^2(t)\,q(t) + \boldsymbol{KN}_{310}p^4(t),
\end{aligned} \tag{75}$$

and the coefficients of the nonlinear stiffnesses (KN_{ij}) are defined in "Appendix A" for the sake of brevity. By employing a dynamic equilibrium technique, the time-dependent terms of the degrees of freedom are written in a series expansion of exponential functions as

$$r_m = \sum_{n=-N}^{N} A_{mn}e^{in\Omega t}, \tag{76}$$

$$p_m = \sum_{n=-N}^{N} B_{mn}e^{in\Omega t}, \tag{77}$$

$$q_m = \sum_{n=-N}^{N} C_{mn}e^{in\Omega t}, \tag{78}$$

and the general dynamic complex equilibrium equations are written as

$$\begin{aligned}
&\left\{-n^2\Omega^2\boldsymbol{M}_{3n\times 3n} + in\Omega\boldsymbol{C}_{3n\times 3n} + \boldsymbol{K}_{3n\times 3n}\right\}\begin{Bmatrix} r_n\\ p_n\\ q_n\end{Bmatrix}_{3n\times 1}\\
&= \begin{Bmatrix} 0\\ 0\\ \boldsymbol{F}_n^{external}(\Omega)\end{Bmatrix}_{3n\times 1} + \begin{Bmatrix} \boldsymbol{KN}1_n^{system}(A_{mn},B_{mn},C_{mn},\Omega)\\ \boldsymbol{KN}2_n^{system}(A_{mn},B_{mn},C_{mn},\Omega)\\ \boldsymbol{KN}3_n^{system}(A_{mn},B_{mn},C_{mn},\Omega)\end{Bmatrix}_{3n\times 1}.
\end{aligned} \tag{79}$$

By solving the discretised coupled $3N$ equations of motion presented in Eq. (79) using a continuation technique [51–53], the nonlinear forced time-dependent mechanical response of the layered hyperelastic structure is obtained.

4 Results and discussion for linear and nonlinear analyses

The coupled motion of shear deformable layered hyperelastic structures is formulated, discretised and solved in the previous sections. In this section, the linear and nonlinear mechanics of the system are analysed and discussed in two main subsections.

4.1 Linear analysis for different shear models

In this subsection, the natural frequencies of the layered hyperelastic structures are analysed and the influence of layering, shear deformation theory and the foundation is discussed in detail.

4.1.1 Model verification

In the first step, in order to verify the current model for analysing layered beam models, the natural frequencies of a three-layered elastic beam structure are obtained for clamped–clamped and pinned–pinned boundaries. Layering is achieved by having steel as the top layer, aluminium in the middle and silicon carbide at the bottom (the elastic material properties of the layers can be found in Ref. [54]), with geometry properties at a length of $L = 2.4$ m, total thickness of $h = 0.03$ m (0.01 m for each layer) and width of $b = 0.12$ m. The first four transverse natural frequencies and the first axial and rotational natural frequencies are obtained using the third-order shear deformable beam theory and compared with those obtained by ANSYS Workbench [55] in Table 1, and the mode shapes are shown in Fig. 2; it can be seen that the current modelling shows great accuracy in computing the natural frequency terms.

4.1.2 Layer sorting, slenderness ratio and shear model effect

Properly layering the structure can have a significant effect in changing the natural frequencies of a hyperelastic beam. To make this possible, three different soft materials are assumed with known Mooney–Rivlin hyperelastic coefficients, as shown in Table 2. For the first step, by assuming a single-layer homogeneous hyperelastic beam with the length of 0.2 mm and nondimensional foundation of $K_L = 1$ and $K_S = 1$, the slenderness ratio ($r = L/h$) is varied and the fundamental natural frequency is obtained for different shear deformation theories in Table 3. It can be seen that for the single-layer model, the fundamental natural frequency of all the five shear models is in good agreement, especially for the vulcanised rubber beam.

By increasing the number of layers to two and three, the fundamental natural frequencies are given in Tables 4 and 5, respectively. It can be seen that by having more than a single layer, the homogeneity in the thickness direction is lost, the coupling terms are considerable and, therefore, the difference between different shear models is slightly more than for the homogeneous single-layer model. Furthermore, it can be seen that for all the layered models and boundary conditions, by increasing the slenderness ratio (L/h), the shear effect loses its importance and the results for different shear models become unique.

Table 1 Linear natural frequencies of a three-layered elastic beam with pinned–pinned and fixed–fixed boundary conditions in hertz

Model	BCs	Transverse				*Axial*	*Rotation*
		Mode 1	Mode 2	Mode 3	Mode 4	Mode 1	Mode 1
Present	*CC*	41.0802	113.129	221.209	365.317	1479.540	2957.979
ANSYS	*CC*	41.322	113.53	221.66	364.64	1482.3	2956.6
Present	*SS*	18.2554	72.9090	163.911	290.543	1479.623	2957.468
ANSYS	*SS*	18.994	72.492	163.67	288.55	1470.2	2955.4

Table 2 Hyperelastic physical properties of soft materials from the literature [56,57]

Material	Mooney Rivlin parameters		
	C_1 (Pa)	C_2 (Pa)	ρ (kg/m^3)
Silicone	253216	4.709e5	1430
Thermoplastic	2.463e5	3.512e6	1152.5
Vulcanised rubber	0.28e6	0.15e6	950

Table 3 Fundamental natural frequencies of *single-layer* hyperelastic beams with different slenderness ratios and shear deformation theories

$r = L/h$	BC	CBT	Timoshenko	Third-Order	Exponential	Trigonometric
Silicone						
100	*CC*	28.1066315	28.1058381	28.0613949	28.0495963	28.0555882
	SS	26.8844497	26.8844452	26.8790424	26.8776181	26.8783409
50	*CC*	20.0984905	20.0909931	19.9747145	19.9433354	19.9592964
	SS	19.0364669	19.0364162	19.0211706	19.0171500	19.0191906
20	*CC*	13.5165344	13.4300982	13.0894529	12.9940148	13.0427443
	SS	12.1552464	12.1540216	12.0947328	12.0790562	12.0870142
10	*CC*	11.0263991	10.6412455	9.97717584	9.78842630	9.88489544
	SS	8.87847552	8.86563176	8.70696574	8.66466219	8.68615087
3D-printed thermoplastic						
100	*CC*	31.8001428	31.7963715	31.5600876	31.4958815	31.5285720
	SS	30.0096747	30.0096449	29.9784623	29.9702373	29.9744119
50	*CC*	23.5675273	23.5423896	23.0001642	22.8473804	22.9255139
	SS	21.3821135	21.3817796	21.2942338	21.2710974	21.2828424
20	*CC*	18.2377203	18.0294260	16.6267951	16.2247058	16.4307878
	SS	14.2187342	14.2109901	13.8816207	13.7934946	13.8382855
10	*CC*	18.5914253	17.4967291	14.9614247	14.21118716	14.5966669
	SS	11.6305988	11.5580599	10.7552375	10.5334826	10.6465584
Vulcanised rubber						
100	*CC*	34.4280536	34.4274664	34.3947866	34.3861353	34.3905276
	SS	32.9775740	32.9775711	32.9736341	32.9725962	32.9731229
50	*CC*	24.5106362	24.5047782	24.4174210	24.3940465	24.4059248
	SS	23.3366630	23.3366304	23.3255149	23.3225840	23.3240715
20	*CC*	16.1341804	16.0555223	15.7864449	15.7121078	15.7499904
	SS	14.8386764	14.8378850	14.7944946	14.7830357	14.7888520
10	*CC*	12.5987291	12.2434931	11.7111708	11.5615479	11.6378881
	SS	10.6887937	10.6803688	10.5628155	10.5316104	10.5474551

4.1.3 Foundation effect

To show the influence of a foundation support on the natural frequencies of layered hyperelastic beams, the structure is assumed to be three-layered with equal thicknesses, ($L/h = 20$) and the foundation terms are varied as $K_L = [0.0, 1.0, 1.0, 3.0, 4.0, 5.0]$ and $K_S = [0.1, 0.2, 0.4, 0.6, 0.8, 1.0]$. The fundamental natural frequencies are shown for both pinned–pinned and clamped–clamped boundary conditions in Tables 6, 7 and 8 for layering as [thermoplastic–silicone–vulcanised rubber], [thermoplastic– vulcanised rubber–silicone] and [silicone–thermoplastic–vulcanised rubber], respectively, using the third-order shear deformable beam model. It can be seen that the layered hyperelastic beam models are more sensitive to variations of the shear term (K_s) compared with the linear term (K_L), and adding the foundation increases the fundamental frequency parameter significantly.

4.2 Nonlinear analysis

The nonlinear dynamics of layered hyperelastic thick beam structures is investigated in this section for various layer, shear and material position models.

Table 4 Fundamental natural frequencies of *two-layered* hyperelastic beams with different slenderness ratios and shear deformation theories

$r = L/h$	BC	CBT	Timoshenko	Third-Order	Exponential	Trigonometric
Sorting: *Silicone–3D-printed thermoplastic*						
100	*CC*	29.7340907	29.7322132	29.6207112	29.5910476	29.6061242
	SS	28.3089814	28.3089689	28.2956561	28.2922077	28.2939558
50	*CC*	21.5192529	21.5058667	21.2413942	21.1685749	21.2057350
	SS	20.0807042	20.0805804	20.0432020	20.0335084	20.0384230
20	*CC*	15.1241626	15.0300170	14.3361165	14.1404376	14.2406520
	SS	12.9733813	12.9710949	12.8278107	12.7904730	12.8094120
10	*CC*	13.3507029	12.9333003	11.5762041	11.1874505	11.3867605
	SS	9.82337237	9.80184612	9.42775842	9.32851239	9.37894002
Sorting: *3D-printed thermoplastic–vulcanised rubber*						
100	*CC*	32.9025718	32.9007381	32.7954063	32.7675713	32.7817124
	SS	31.3673283	31.3673136	31.3551669	31.3520513	31.3536296
50	*CC*	23.7164675	23.7035445	23.4548446	23.3868036	23.4215140
	SS	22.2348245	22.2346909	22.2007027	22.1919742	22.1963967
20	*CC*	16.3475598	16.2654456	15.6174109	15.4361428	15.528951
	SS	14.2969492	14.2950743	14.1652090	14.1317878	14.1487259
10	*CC*	13.9084386	13.5779696	12.2872118	11.9217392	12.1090495
	SS	10.6682708	10.6525061	10.3088192	10.2191370	10.2646474
Sorting: *Vulcanised rubber–silicone*						
100	*CC*	30.7828884	30.7822099	30.7442483	30.7341990	30.7393013
	SS	29.4676038	29.4676004	29.4630306	29.4618281	29.4624383
50	*CC*	21.9580668	21.9515018	21.8512018	21.8242796	21.8379663
	SS	20.8582540	20.8582149	20.8453158	20.8419207	20.8436436
20	*CC*	14.5905007	14.5104299	14.2102543	14.1267312	14.1693410
	SS	13.2865750	13.2856309	13.2353502	13.2220888	13.2288196
10	*CC*	11.6111038	11.2593795	10.6693876	10.5025821	10.5877820
	SS	9.62848313	9.61850920	9.48290029	9.44689586	9.46517866

Table 5 Fundamental natural frequencies of *three-layered* hyperelastic beams with different slenderness ratios and shear deformation theories

$r = L/h$	BC	CBT	Timoshenko	Third-Order	Exponential	Trigonometric
Sorting: *Silicone–3D-printed thermoplastic– vulcanised rubber*						
100	*CC*	30.9681123	30.9677558	30.9280699	30.917347	30.9228017
	SS	29.6263359	29.6263339	29.6215268	29.620237	29.6208931
50	*CC*	22.1334388	22.1300004	22.0257725	21.997078	22.0116995
	SS	20.9763997	20.9763776	20.9628076	20.959166	20.9610175
20	*CC*	14.8485713	14.8065505	14.5019297	14.413923	14.4587790
	SS	13.3871531	13.3866154	13.3336929	13.319438	13.3266873
10	*CC*	12.052601	9211.8570456	11.2633773	11.084178	9.11.1761513
	SS	9.76211837	9.75638969	9.61347065	9.574479	48 9.59432579
Sorting: *3D-printed thermoplastic–silicone– vulcanised rubber*						
100	*CC*	31.0792240	31.0771291	30.9822274	30.957249	9.30.9699350
	SS	29.6369342	29.6369169	29.6262028	29.623464	5 29.6248515
50	*CC*	22.3854567	22.3707232	22.1464147	22.085406	2 22.1165090
	SS	21.0057928	21.0056361	20.9756990	20.968037	0 20.9719186
20	*CC*	15.3767687	15.2849197	14.6992985	14.536124	14.6199287
	SS	13.4959180	13.4938098	13.3798142	13.350614	4 13.3654096
10	*CC*	12.9909881	12.6319641	11.4549604	11.128466	6 11.2954731
	SS	10.0454782	10.0282134	9.72613705	9.648189	929.68770610
Sorting: *3D-printed thermoplastic–vulcanised rubber–silicone*						
100	*CC*	31.1189765	31.1164982	31.0054465	30.976079	1 30.9909968
	SS	29.6422094	29.6421922	29.6292289	29.625888	6 29.6275813
50	*CC*	22.4882142	22.4706799	22.205782	0 22.133457	5 22.1703283
	SS	21.0208307	21.0206653	20.9843036	20.974924	0 20.9796777
20	*CC*	15.6954145	15.5768274	14.8707311	14.673673	3 14.7744629
	SS	13.5560659	13.5532475	13.4139315	13.377907	2 13.3961688
10	*CC*	13.6707649	13.1694255	11.7529818	11.358212	5 11.5600729
	SS	10.2074657	10.1817722	9.81514643	9.719439	329.76798865

Table 6 Fundamental natural frequencies of three-layered hyperelastic beams [*thermoplastic–silicone–vulcanised rubber*] with different slenderness ratios and shear deformation theories

	$K_S = 0.1$	$K_S = 0.2$	$K_S = 0.4$	$K_S = 0.6$	$K_S = 0.8$	$K_S = 1.0$
Pinned–pinned						
$K_L = 0.0$	4.44576163	5.97334523	8.21583078	9.96541025	11.4504844	12.7637935
$K_L = 1.0$	5.98912959	7.19623324	9.14356823	10.7431088	12.1333669	13.3798142
$K_L = 2.0$	7.20933731	8.23958051	9.98547942	11.4681894	12.7798116	13.9686945
$K_L = 3.0$	8.25102479	9.16491111	10.7617263	12.1500759	13.3950951	14.5337338
$K_L = 4.0$	9.17519864	10.0050236	11.4856302	12.7956757	13.9833313	15.0776128
$K_L = 5.0$	10.0144457	10.7798607	12.1665379	13.4102305	14.5478016	15.6025444
Fixed–fixed						
$K_L = 0.0$	6.06990371	7.46126469	9.61553921	11.3408049	12.8222314	14.1412529
$K_L = 1.0$	7.27559657	8.47125334	10.4188043	12.0294404	13.4351646	14.6992985
$K_L = 2.0$	8.30811966	9.37303420	11.1644234	12.6807332	14.0213286	15.2369188
$K_L = 3.0$	9.22579923	10.1953607	11.8632707	13.3001703	14.5839514	15.7562049
$K_L = 4.0$	10.0601124	10.9561383	12.5231789	13.8920136	15.1256604	16.2589136
$K_L = 5.0$	10.8303428	11.6674130	13.1500116	14.4596519	15.6486275	16.7465377

Table 7 Fundamental natural frequencies of three-layered hyperelastic beams [*thermoplastic–vulcanised rubber–silicone*] with different slenderness ratios and shear deformation theories

	$K_S = 0.1$	$K_S = 0.2$	$K_S = 0.4$	$K_S = 0.6$	$K_S = 0.8$	$K_S = 1.0$
Pinned–pinned						
$K_L = 0.0$	4.56023487	6.05767609	8.27569748	10.0136505	11.4915612	12.7998710
$K_L = 1.0$	6.07392035	7.26582713	9.19695668	10.7874954	12.1718053	13.4139315
$K_L = 2.0$	7.27937245	8.29994197	10.0339844	11.5094268	12.8159938	14.0010860
$K_L = 3.0$	8.31179923	9.21877531	10.8063715	12.1886727	13.4293164	14.5645889
$K_L = 4.0$	9.22944950	10.0539837	11.5271191	12.8320134	14.0158257	15.1070870
$K_L = 5.0$	10.0637695	10.8249409	12.2053789	13.4446043	14.5787582	15.6307676
Fixed–fixed						
$K_L = 0.0$	6.46909276	7.78987081	9.87438670	11.5620699	13.0187251	14.3196948
$K_L = 1.0$	7.61113810	8.76148587	10.6577014	12.2378694	13.6224732	14.8707311
$K_L = 2.0$	8.60288588	9.63561855	11.3872584	12.8782530	14.2005746	15.4020647
$K_L = 3.0$	9.49156616	10.4367915	12.0728072	13.4882660	14.7560438	15.9156689
$K_L = 4.0$	10.3038813	11.1807000	12.7214645	14.0718587	15.2913474	16.4132083
$K_L = 5.0$	11.0566755	11.8781081	13.3386134	14.6321926	15.8085341	16.8961020

Table 8 Fundamental natural frequencies of three-layered hyperelastic beams [*silicone–thermoplastic–vulcanised rubber*] with different slenderness ratios and shear deformation theories

	$K_S = 0.1$	$K_S = 0.2$	$K_S = 0.4$	$K_S = 0.6$	$K_S = 0.8$	$K_S = 1.0$
Pinned–pinned						
$K_L = 0.0$	4.31840975	5.87720585	8.14415800	9.90520367	11.3973154	12.7155232
$K_L = 1.0$	5.89504178	7.11648799	9.07910558	10.6871841	12.0831138	13.3336929
$K_L = 2.0$	7.13122503	8.16989914	9.92637922	11.4157236	12.7320257	13.9244461
$K_L = 3.0$	8.18273922	9.10220306	10.7068131	12.1004787	13.3494312	14.4911363
$K_L = 4.0$	9.11372973	9.94750958	11.4341021	12.7485067	13.9395175	15.0364843
$K_L = 5.0$	9.95805785	10.7264062	12.1178187	13.3651509	14.5056189	15.5627340
Fixed–fixed						
$K_L = 0.0$	5.76095561	7.19395301	9.38000579	11.1192680	12.6096991	13.9357624
$K_L = 1.0$	7.02042195	8.23721111	10.2021634	11.8210913	13.2327187	14.5019297
$K_L = 2.0$	8.08603946	9.16244126	10.9628357	12.4835201	13.8276959	15.0468088
$K_L = 3.0$	9.02672360	10.0024501	11.6740478	13.1125264	14.3981075	15.5726343
$K_L = 4.0$	9.87823054	10.7771835	12.3443516	13.7127101	14.9467664	16.0812756
$K_L = 5.0$	10.6619479	11.4998415	12.9800861	14.2877041	15.4759861	16.5743147

4.2.1 Comparison of different shear models

Five different shear deformable beam theories were used in previous sections for modelling and formulation of the layered hyperelastic beam structure. In this section, the amplitude response of the sandwich structure for different shear models is examined. Three layers are assumed, and the thickness of the layers is assumed as $h = [h/4, h/2, h/4]$ with $L/h = 10$, $K_L = K_{NL} = 1$, $K_s = 0.1$, with the material sorting as [silicone–vulcanised rubber–thermoplastic]. In the first step, the influence of considering the shear effect as negligible (CBT), linear (Timoshenko) or higher order (third order) is examined, and the axial, transverse and rotation amplitudes are obtained, as shown in Figs. 3, 4 and 5 for *clamped–clamped* and Figs. 6, 7 and 8 for *pinned–pinned* boundary conditions. It can be seen that for both boundary conditions, the Timoshenko beam model gives the highest maximum amplitude for the dominant axial, transverse and rotation deformation. Furthermore, increasing the shear effect from the linear model to higher-order moves the resonance peak to lower frequencies.

The influence of using different types of higher-order shear deformable theories on the amplitude response is investigated for the similar three-layered hyperelastic beams with the given properties. Figures 9, 10, 11, 12, 13 and 14 show the axial, transverse and rotation amplitudes of *clamped–clamped* and *pinned–pinned* thick beam models, respectively. The results for the different higher-order shear models are fairly in good agreement, especially for the pinned–pinned boundary condition. Comparing the amplitude response of the dominant terms of axial, transverse and rotation motions, it can be seen that the highest amplitude is for the third-order beam model and the lowest belongs to the exponential beam model.

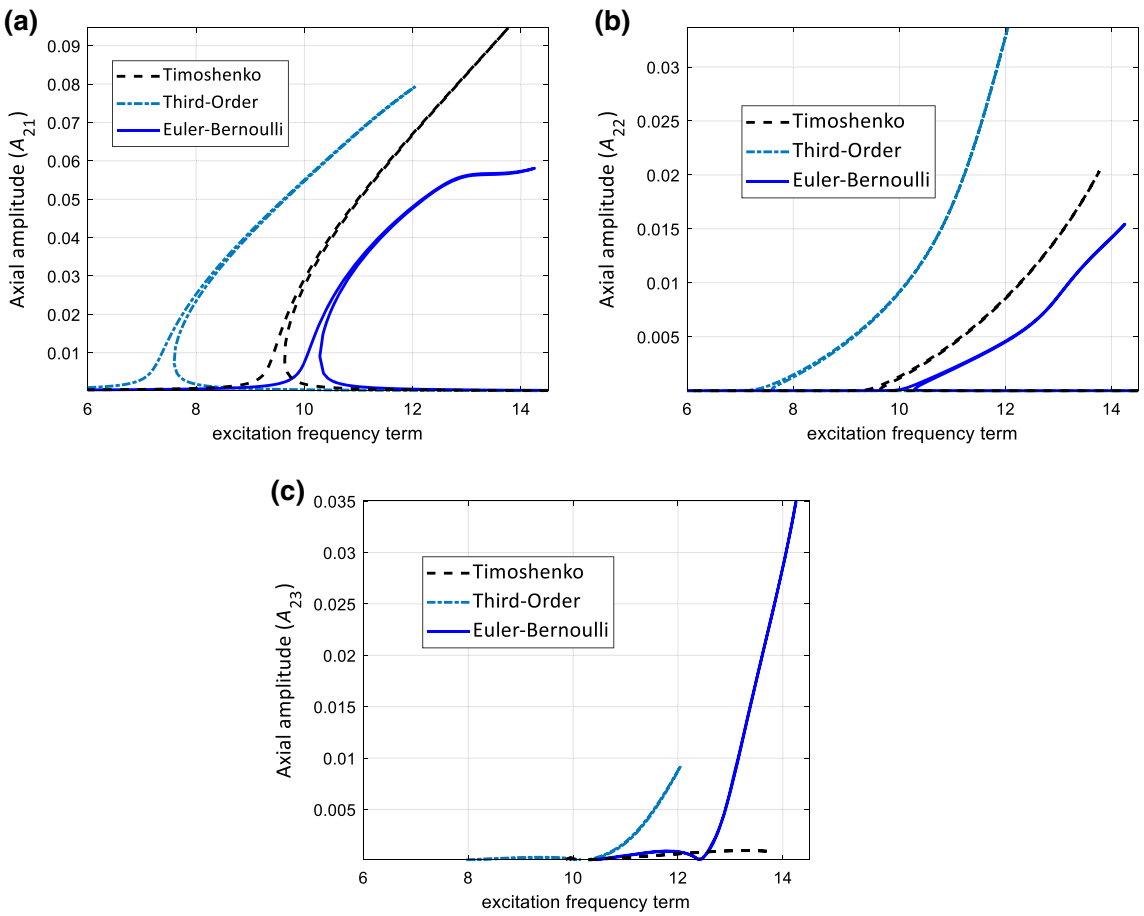

Fig. 3 Influence of considering shear effect on the *axial* amplitude response of the sandwich hyperelastic *clamped–clamped* beam **a** A_{21}, **b** A_{22} and **c** A_{23}

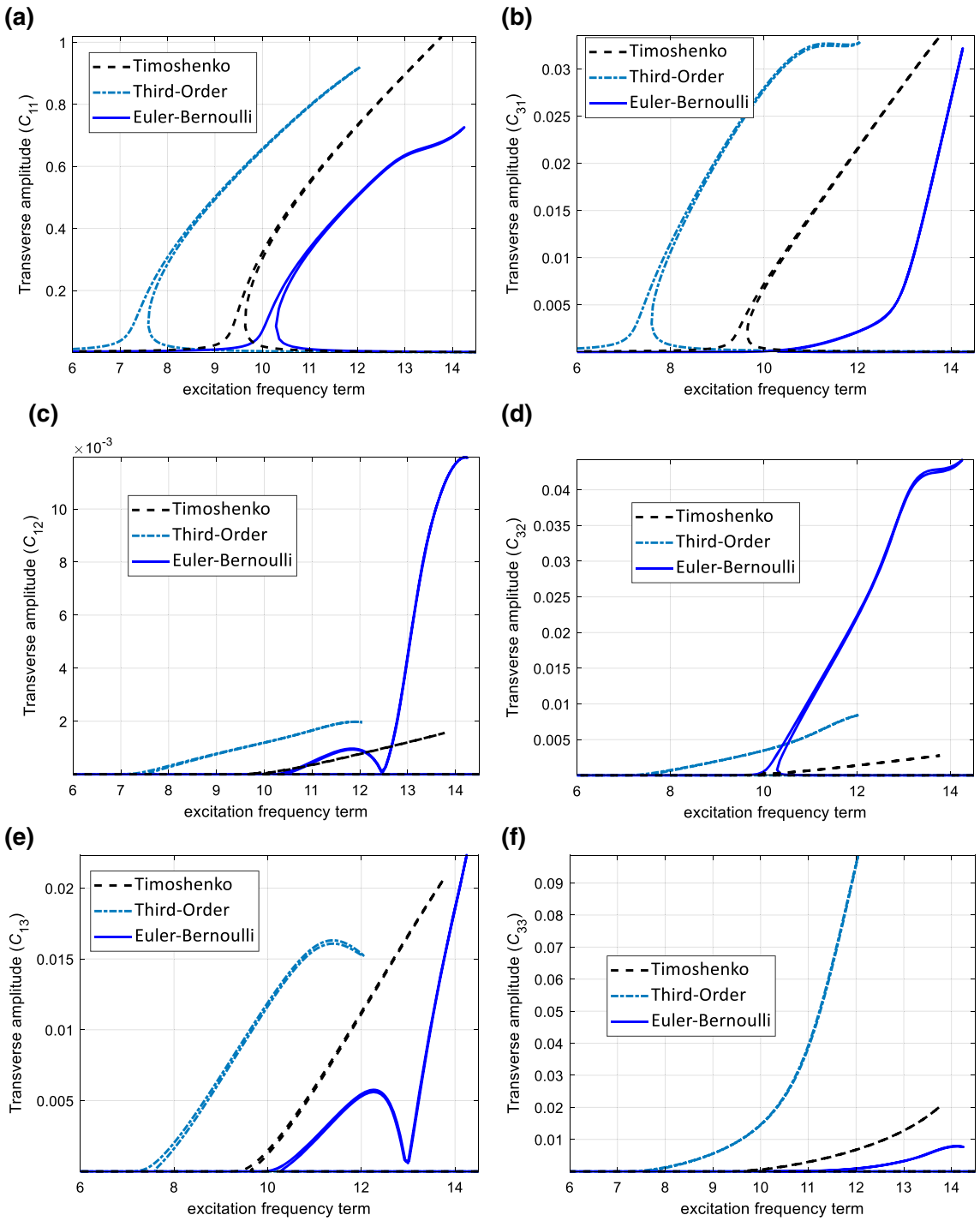

Fig. 4 Influence of considering shear effect on the *transverse* amplitude response of the sandwich hyperelastic *clamped–clamped* beam **a** C_{11}, **b** C_{31}, **c** C_{12}, **d** C_{32}, **e** C_{13}, and **f** C_{33}

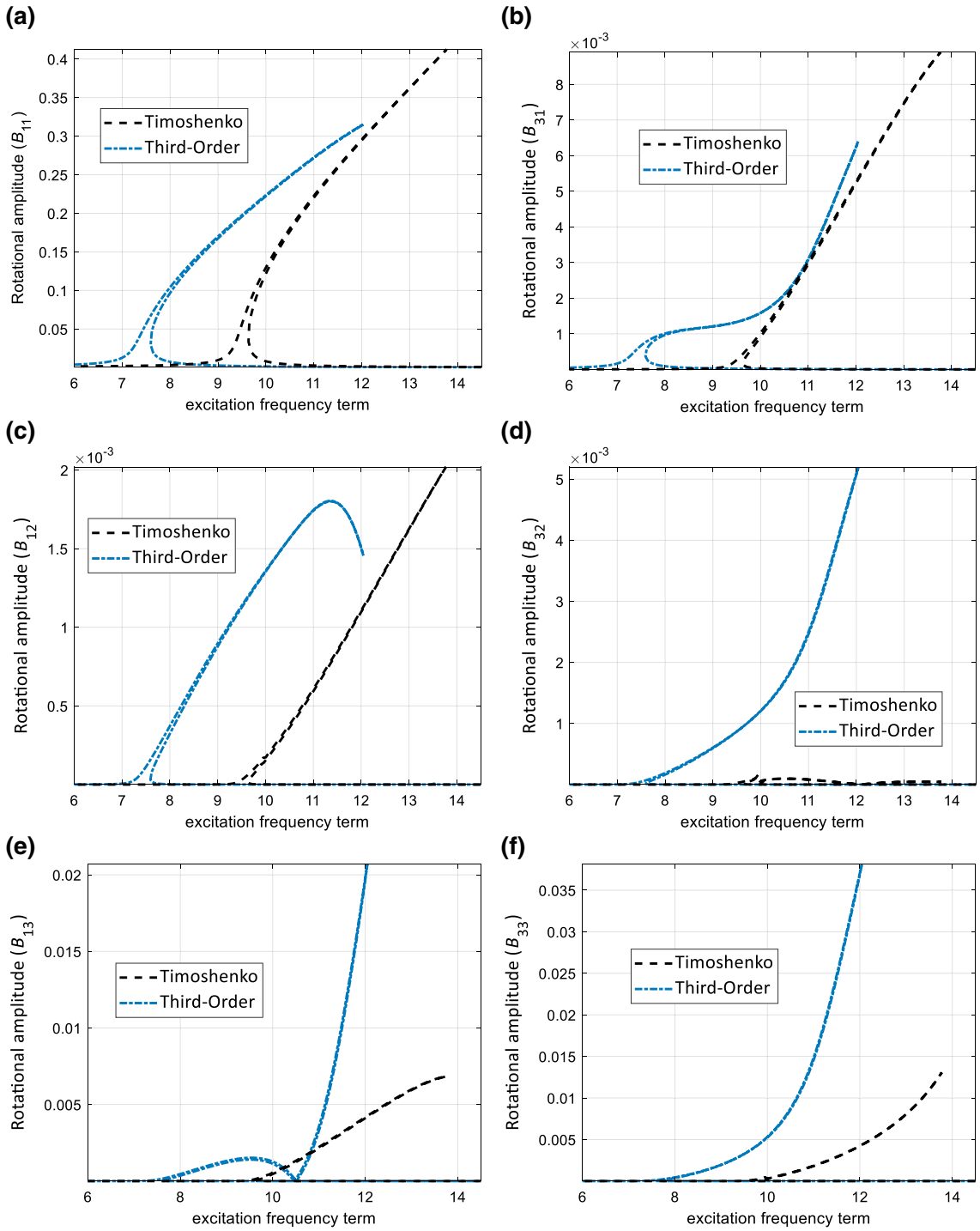

Fig. 5 Influence of considering shear effect on the *rotation* amplitude response of the sandwich hyperelastic *clamped–clamped* beam **a** B_{11}, **b** B_{31}, **c** B_{12}, **d** B_{32}, **e** B_{13}, and **f** B_{33}

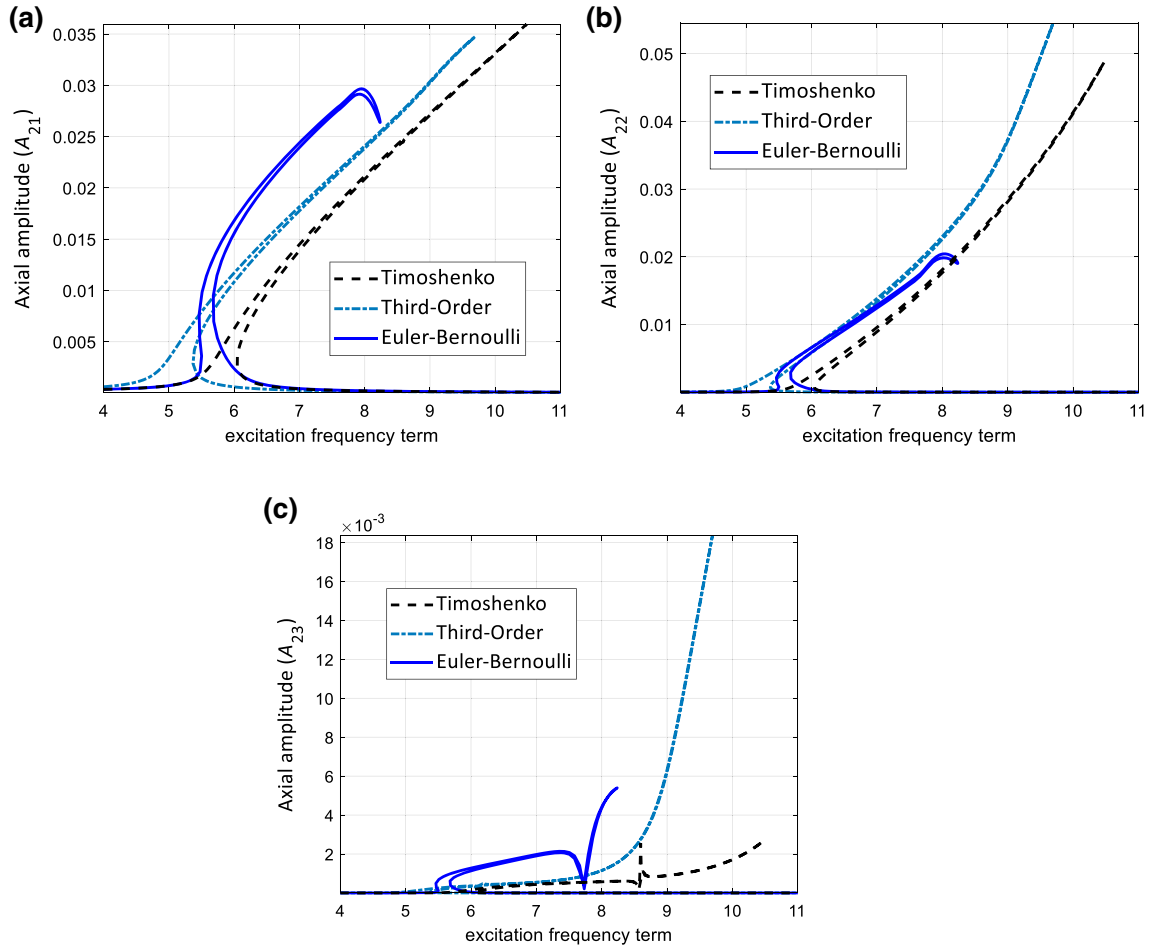

Fig. 6 Influence of considering shear effect on the *axial* amplitude response of the sandwich hyperelastic *pinned–pinned* beam **a** A_{21}, **b** A_{22} and **c** A_{23}

4.2.2 Influence of layering

Layering a hyperelastic structure for different purposes can change the dynamic behaviour of the structure significantly. In Sect. 4.1.1., this influence on the linear vibration response is analysed, and in this section, the nonlinear vibration response of the structure based on the number of layers is examined. To this end, for a homogeneous single-layer structure, the dominant amplitude responses are shown in Fig. 15, for thermoplastic, vulcanised rubber and silicone hyperelastic thick beams using the third-order shear deformable beam theory model. It can be seen that thermoplastic and silicone show a stiffness hardening effect, while the vulcanised rubber beam model shows a drop in the amplitude response of the axial motion while increasing the frequency and continues to go up afterwards.

By increasing the layers to two by having $h_1 = h_2 = h/2$, the dominant longitudinal, transverse and rotation amplitude responses of the structure are shown for different hyperelastic materials in Fig. 16 for a combination of different hyperelastic materials which the combination is given as Mat = ([*mat*1- *mat*2], [*mat*1- *mat*3], [*mat*2- *mat*3]) with *mat*1 = *thermoplastic*, *mat*2 = *silicone*, *mat*3 = *vulcanised rubber*. It can be seen that the highest transverse amplitude belongs to the material combination of [*mat*2- *mat*3], while the other two models have almost the same behaviour.

Finally, by having three layers ($h_1 = h_2 = h_3 = h/3$) and varying the layers as Mat = ([*mat*1-*mat*2-*mat*3], [*mat*2-*mat*1-*mat*3], [*mat*1-*mat*3-*mat*2]), the dominant amplitude responses of the longitudinal, transverse and rotation motions are shown in Fig. 17. It can be seen that the material distribution [*mat*2- *mat*1- *mat*3] has the lowest maximum axial amplitude and the highest transverse and rotation amplitudes; this shows that for

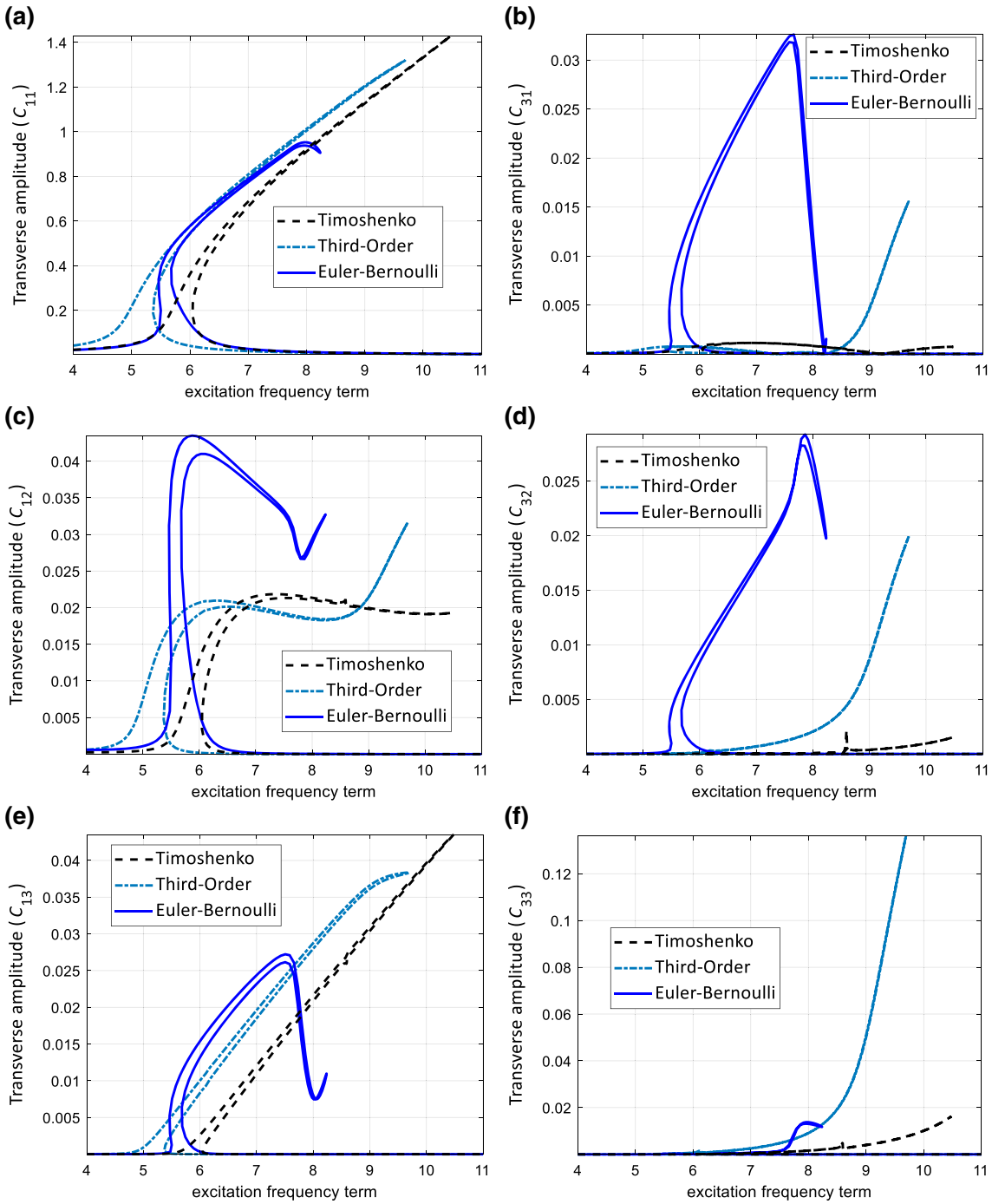

Fig. 7 Influence of considering shear effect on the *transverse* amplitude response of the sandwich hyperelastic *pinned–pinned* beam **a** C_{11}, **b** C_{31}, **c** C_{12}, **d** C_{32}, **e** C_{13} and **f** C_{33}

the other two material models, the coupling between the axial and transverse motion is noticeably higher and should be considered.

4.2.3 Influence of layer thickness

Changing the thickness of the layers can change the nonlinear vibration response of the structure significantly. To show this influence, the material distribution is Mat = [*mat*1-*mat*2-*mat*3] and the thickness of layers are

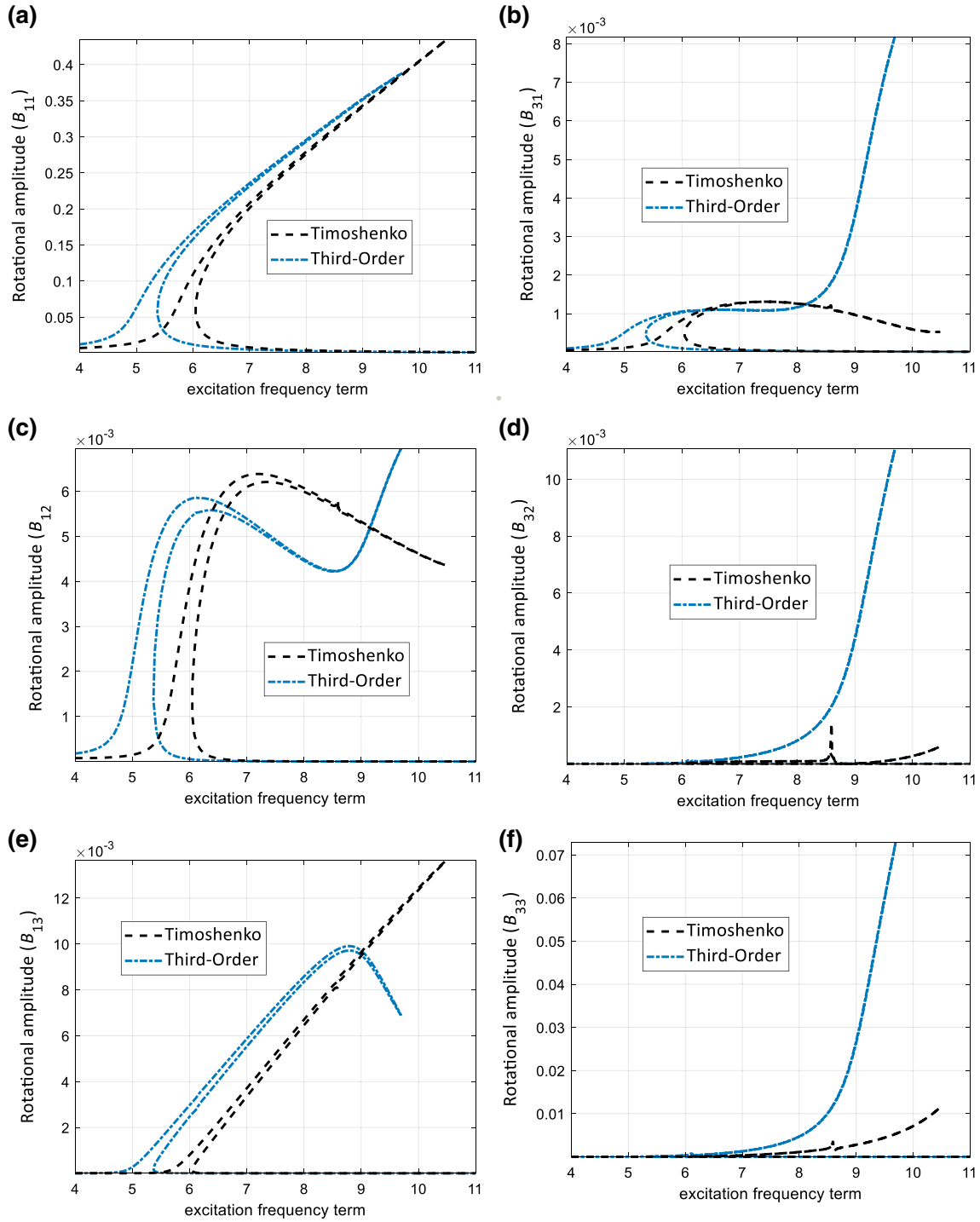

Fig. 8 Influence of considering shear effect on the *rotation* amplitude response of the sandwich hyperelastic *pinned–pinned* beam **a** B_{11}, **b** B_{31}, **c** B_{12}, **d** B_{32}, **e** B_{13} and **f** B_{33}

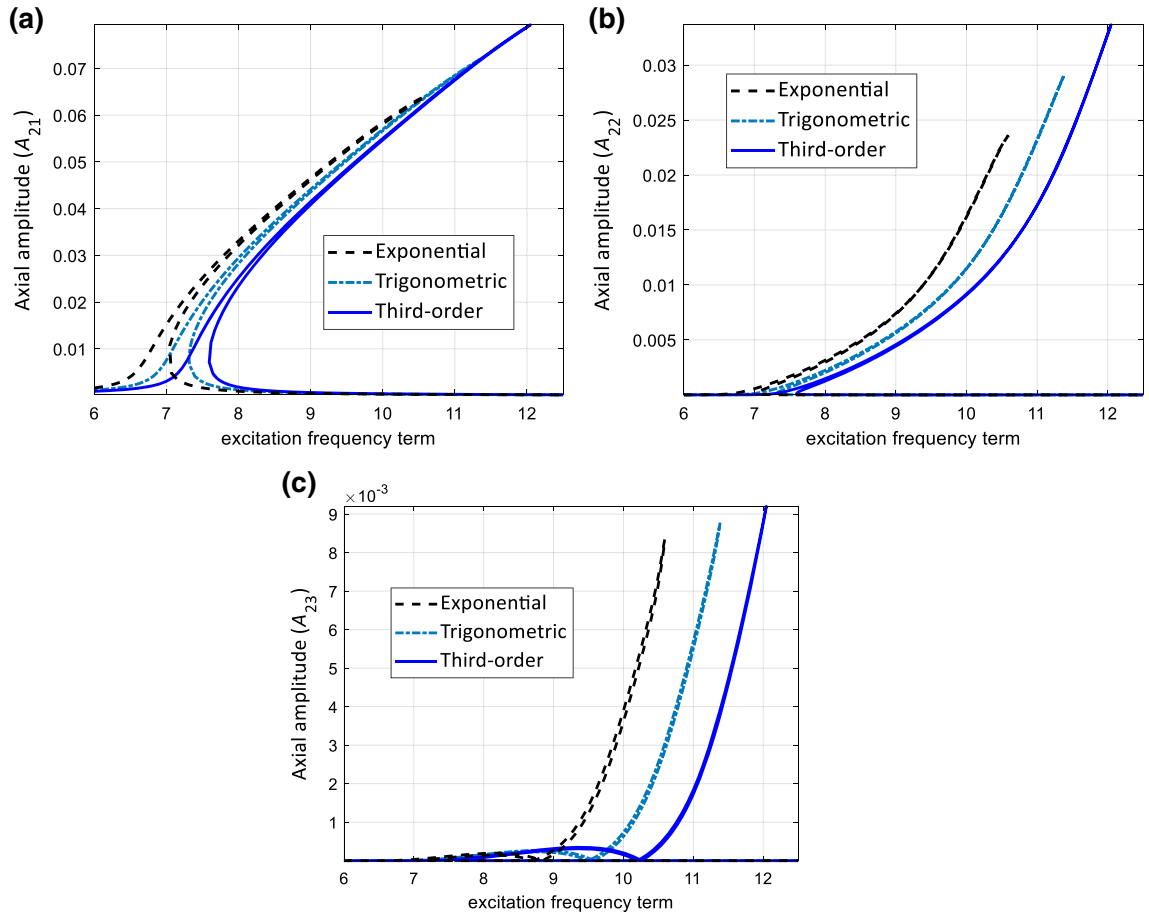

Fig. 9 Influence of different higher-order shear effect models on the *axial* amplitude response of the sandwich hyperelastic *clamped–clamped* beam **a** A_{21}, **b** A_{22}, and **c** A_{23}

$h = ([h/4, h/4, h/2], [h/2\,h/4, h/4], [h/4, h/2, h/4])$. The frequency–amplitude response of the structure is plotted in Figs. 18, 19 and 20 for axial, transverse and rotation deformations, respectively. It can be seen that changing the thickness of the layers has a significant effect in varying the nonlinear behaviour of the system. Besides, the maximum amplitude of all the deformation coordinates moves to higher frequencies for $h = [h/2, h/4, h/4]$ and the other two models show similar behaviour in dominant amplitude coordinates.

4.2.4 Influence of material positioning

To show the importance of the position of the hyperelastic material in a layered structure, a three-layered beam is assumed with the thickness of $h = [h/4, h/2, h/4]$ which shows that the middle layer (the core) is thicker than the outer layers. In this section, by varying the materials in the layers, the nonlinear forced vibration response of the system is studied. To do this, the position of the material is varied and the dominant amplitude–frequency responses in axial, transverse and rotation motions of the structure are shown in Figs. 21 and 22 for pinned–pinned and clamped–clamped conditions, respectively. It can be seen that for both boundary conditions, the maximum amplitudes sweep to lower frequencies when the material positioning is [*mat*1-*mat*2-*mat*3]; the clamped–clamped and pinned-pinned beam models show that the dominant rotation coordinate reaches its highest when the material positioning is [*mat*1-*mat*2-*mat3*].

4.2.5 Influence of layer positioning

Another important goal of this study is to show the influence of layering and positioning the layers in manufacturing sandwich hyperelastic structures. To demonstrate this effect, the position of the layers is varied with

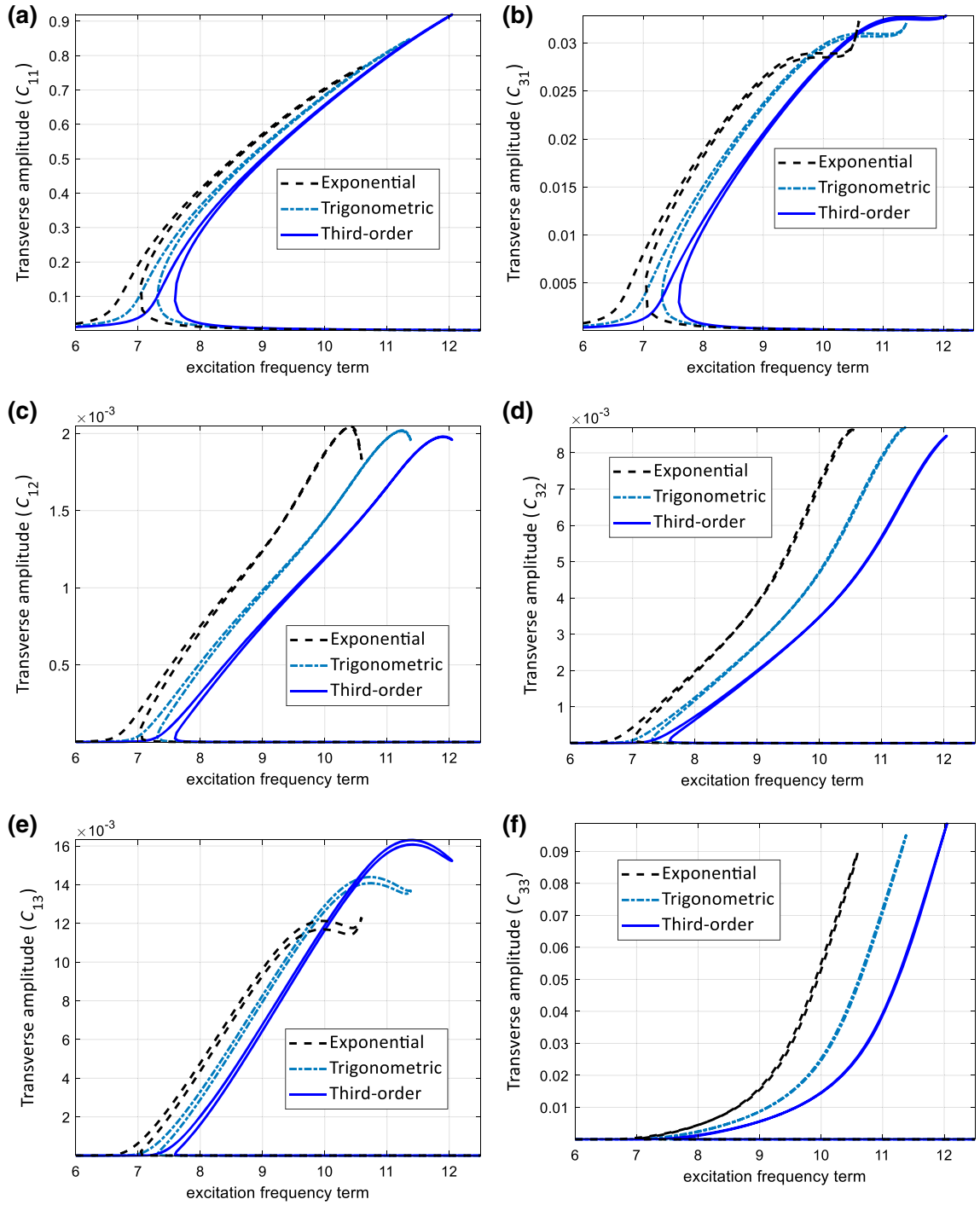

Fig. 10 Influence of different higher-order shear effect models on the *transverse* amplitude response of the sandwich hyperelastic *clamped–clamped* beam **a** C_{11}, **b** C_{31}, **c** C_{12}, **d** C_{32}, **e** C_{13}, and **f** C_{33}

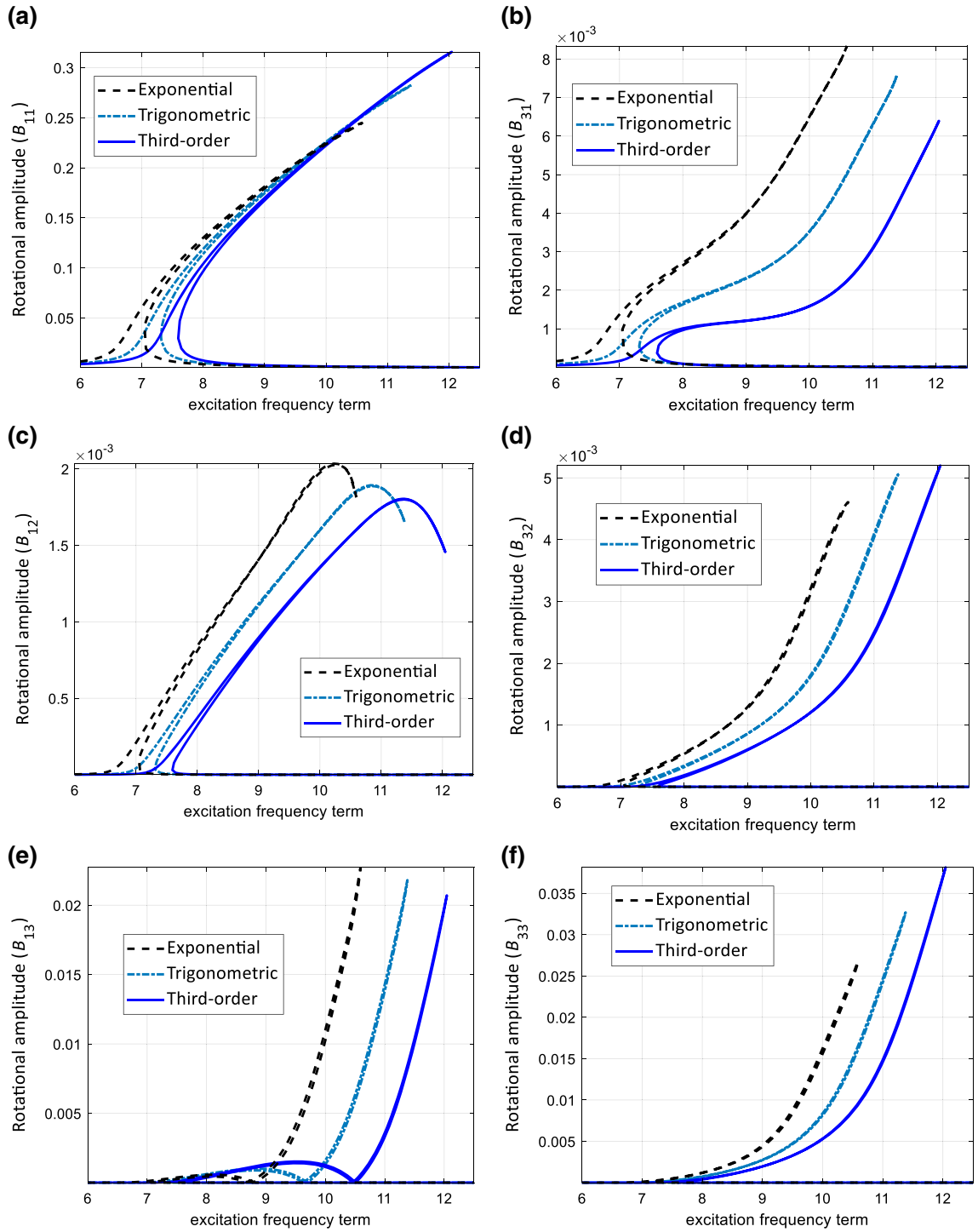

Fig. 11 Influence of different higher-order shear effect models on the *rotation* amplitude response of the sandwich hyperelastic *clamped–clamped* beam **a** B_{11}, **b** B_{31}, **c** B_{12}, **d** B_{32}, **e** B_{13} and **f** B_{33}

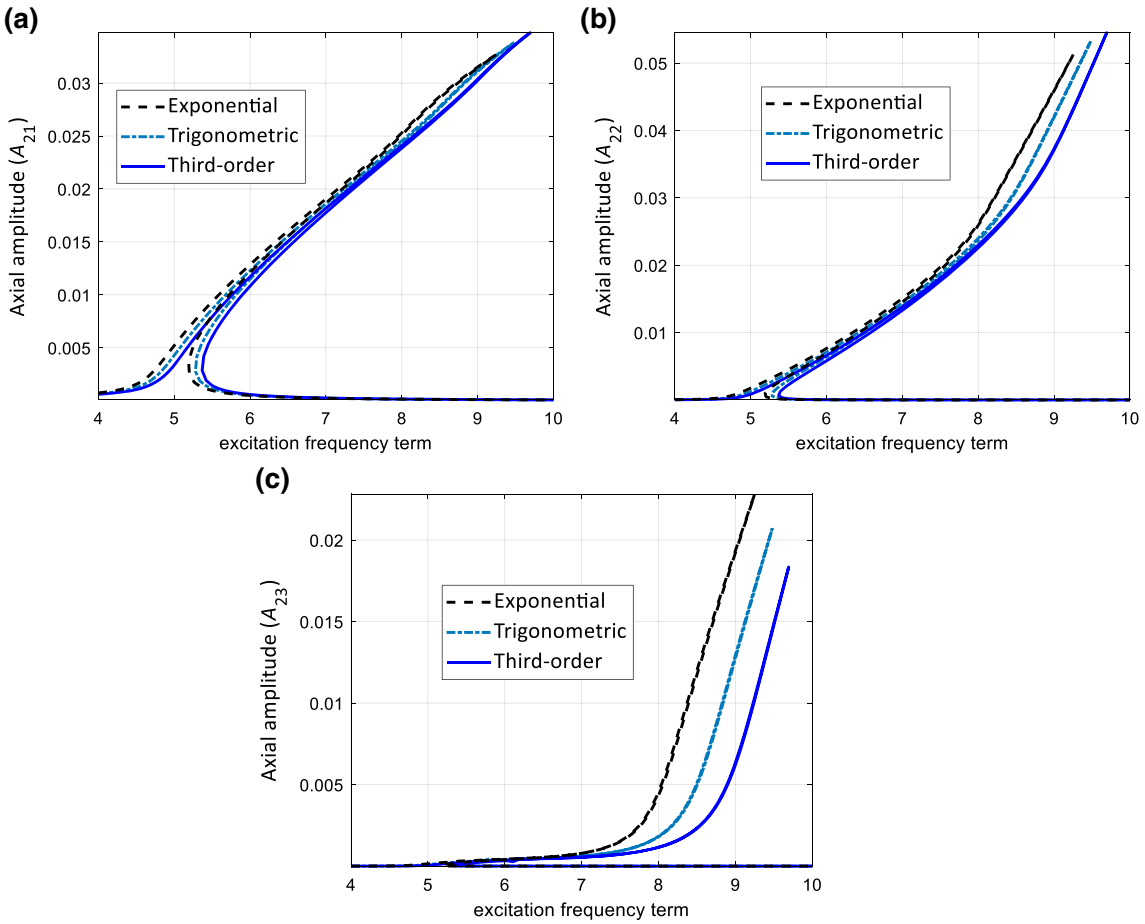

Fig. 12 Influence of different higher-order shear effect models on the *axial* amplitude response of the sandwich hyperelastic *pinned–pinned* beam **a** A_{21}, **b** A_{22} and **c** A_{23}

the thickness of $h = [h/4, h/2, h/4]$ and the amplitude–frequency responses of the structures are shown in Figs. 23, 24 and 25 for clamped–clamped third-order shear deformable hyperelastic thick beams. It can be seen that the layer positioning has a notable effect in changing the coupling motion of the structure, based on the requirements of the design.

5 Summary and conclusions

In this study, a detailed layerwise analysis of the time-dependent mechanics of hyperelastic beams structures is given using five different shear deformation theories. The hyperelasticity was modelled following the Mooney–Rivlin hyperelastic strain energy density model, and the beam was assumed to lie on a foundation including linear, nonlinear and shear layers. Equations of motion were derived using Hamilton's principle together with different shear deformable beam theories. Solving the equations of motion using a dynamic equilibrium technique, it was shown that:

- The classic beam theory predicts the fundamental frequency term of hyperelastic-layered beam models higher than the studied shear deformable beam models.
- By increasing the length-to-thickness ratio, the influence of the type of boundary conditions decreases.
- Similar to elastic beams, the hyperelastic-layered beam model shows higher sensitivity to shear effects when the length-to-thickness ratio is lower.
- The higher-order shear deformable beam models (namely third-order, exponential and trigonometric) give very close results for natural frequency terms, while the nonlinear behaviours are slightly different.

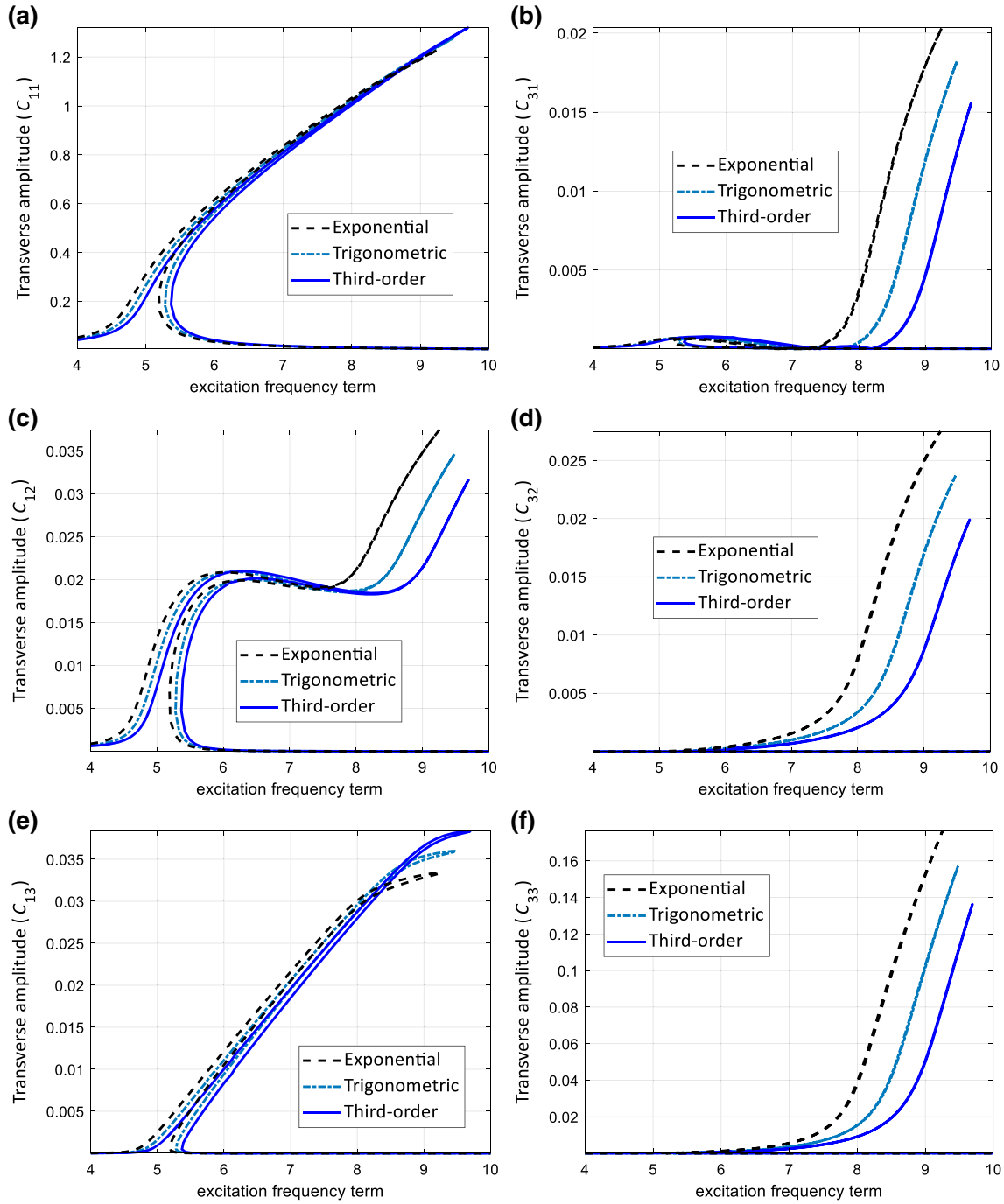

Fig. 13 Influence of different higher-order shear effect models on the *transverse* amplitude response of the sandwich hyperelastic *pinned–pinned* beam **a** C_{11}, **b**)C_{31}, **c** C_{12}, **d** C_{32}, **e** C_{13} and **f** C_{33}

- For linear natural frequencies, it was shown that having a foundation can increase the fundamental natural frequency of hyperelastic-layered beams significantly and this effect is higher for the shear layer compared with the linear layer.
- For nonlinear forced time-dependent analysis of layered hyperelastic beams, the Timoshenko beam model gives the highest maximum amplitude for the dominant longitudinal, transverse and rotation deformations, compared with the other shear deformable models. Similarly, for higher-order shear models, the highest amplitudes are for the third-order beam model and the lowest one belongs to the exponential beam model.

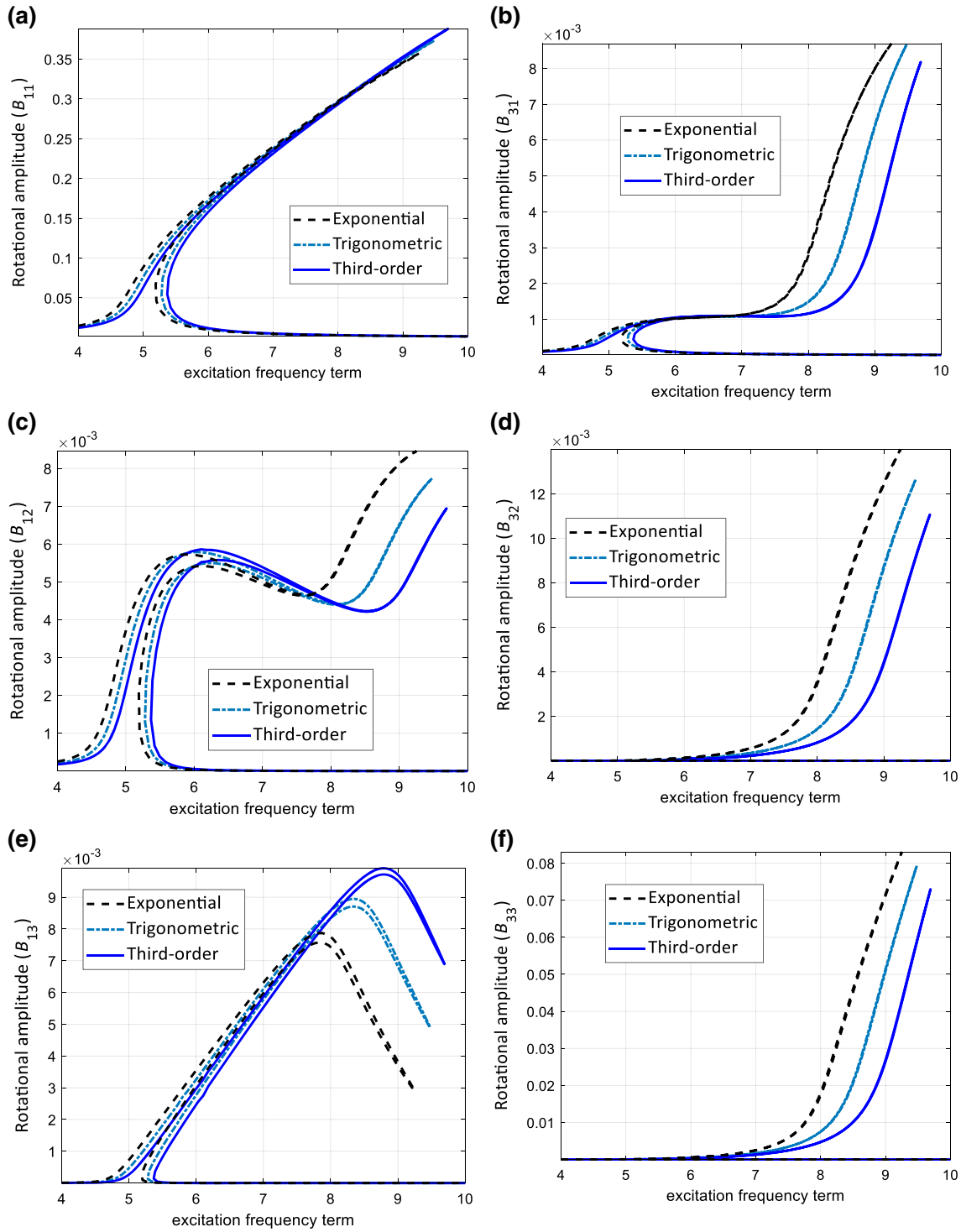

Fig. 14 Influence of different higher-order shear effect models on the *rotation* amplitude response of the sandwich hyperelastic *pinned–pinned* beam **a** B_{11}, **b** B_{31}, **c** B_{12}, **d** B_{32}, **e** B_{13} and **f** B_{33}

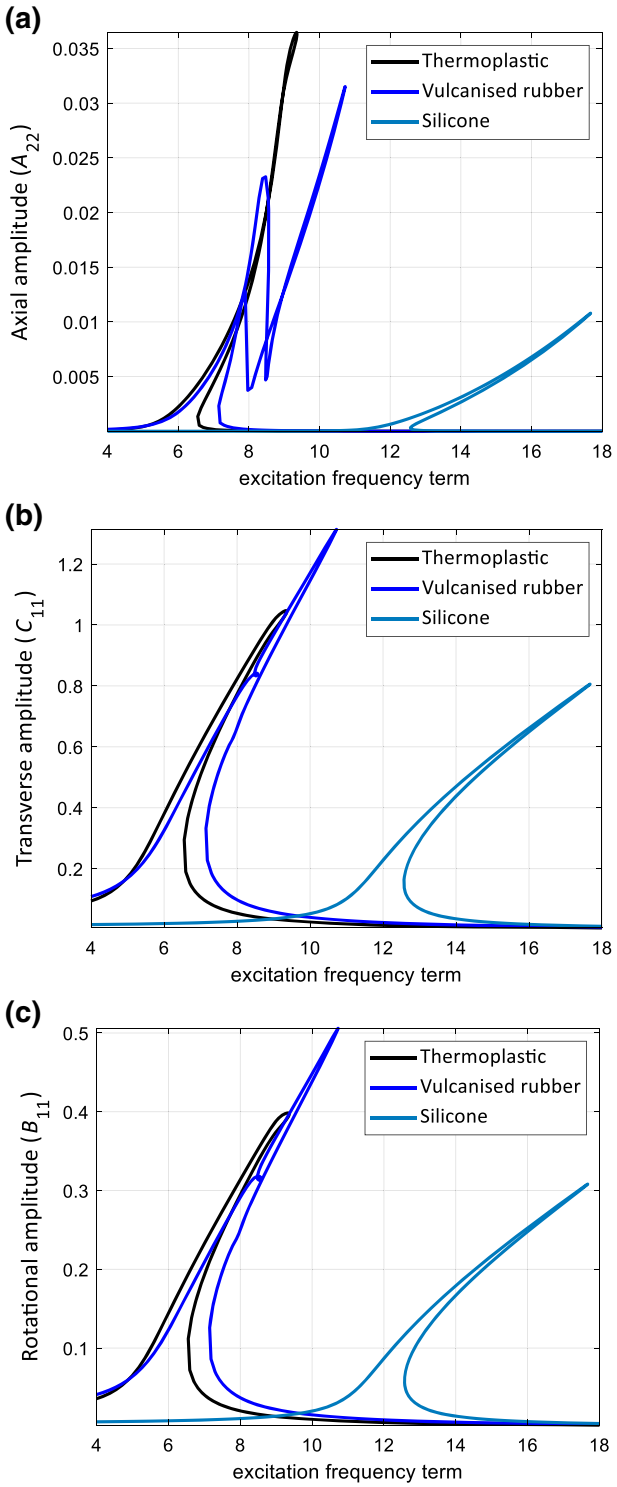

Fig. 15 The amplitude response of the *single-layer* hyperelastic *clamped–clamped* beam **a** A_{22}, **b** C_{11}, **c** B_{11}

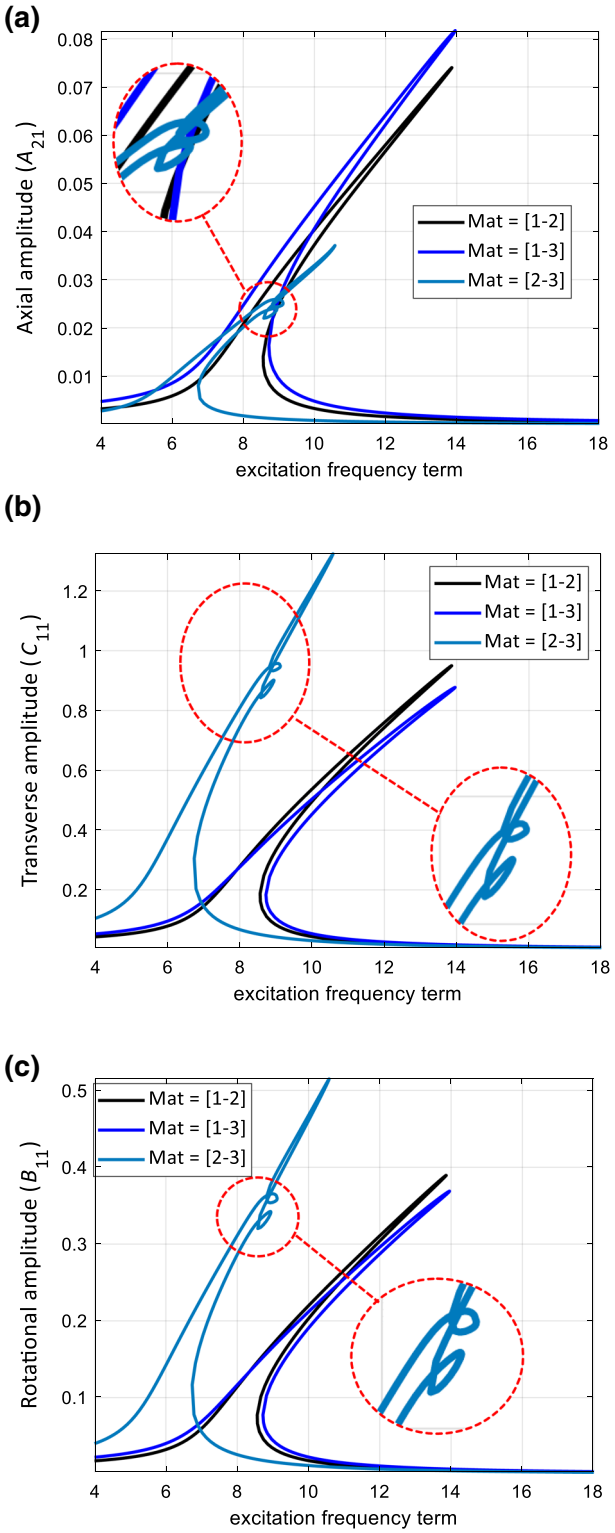

Fig. 16 The amplitude response of the *two-layered* hyperelastic *clamped–clamped* beam **a** A_{21}, **b** C_{11}, **c** B_{11}

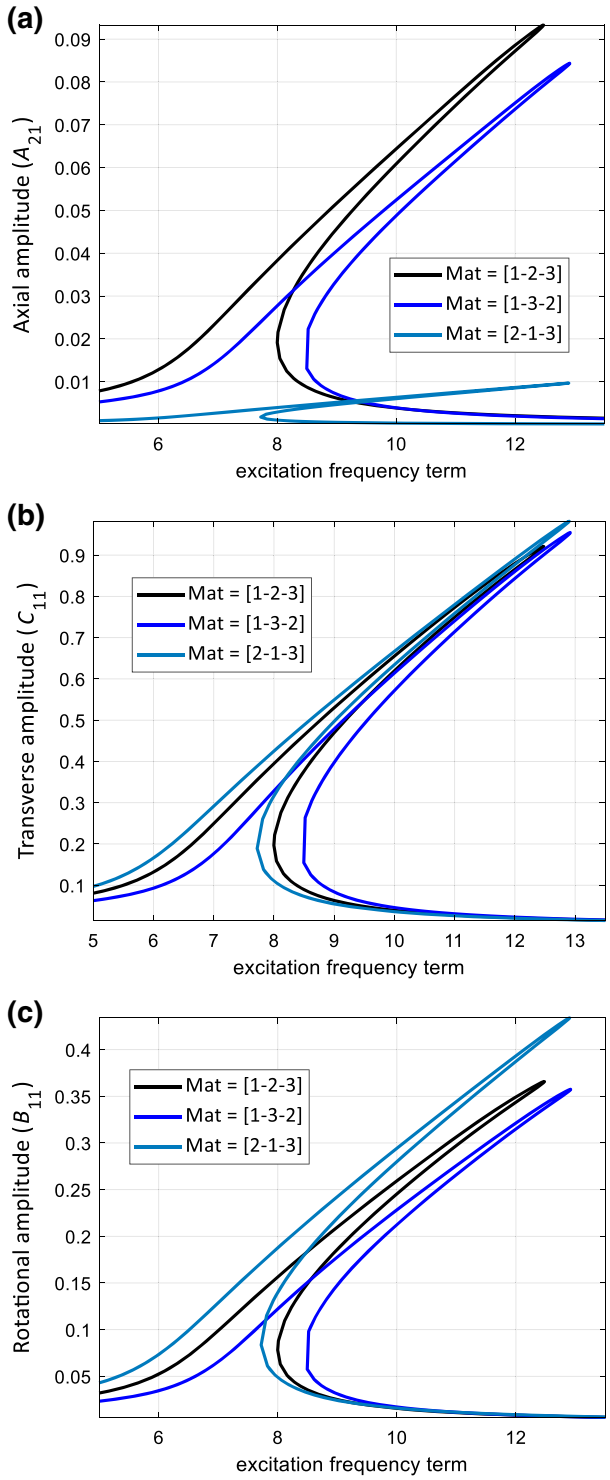

Fig. 17 The amplitude response of the *three-layered* hyperelastic *clamped–clamped* beam **a** A_{21}, **b** C_{11}, **c** B_{11}

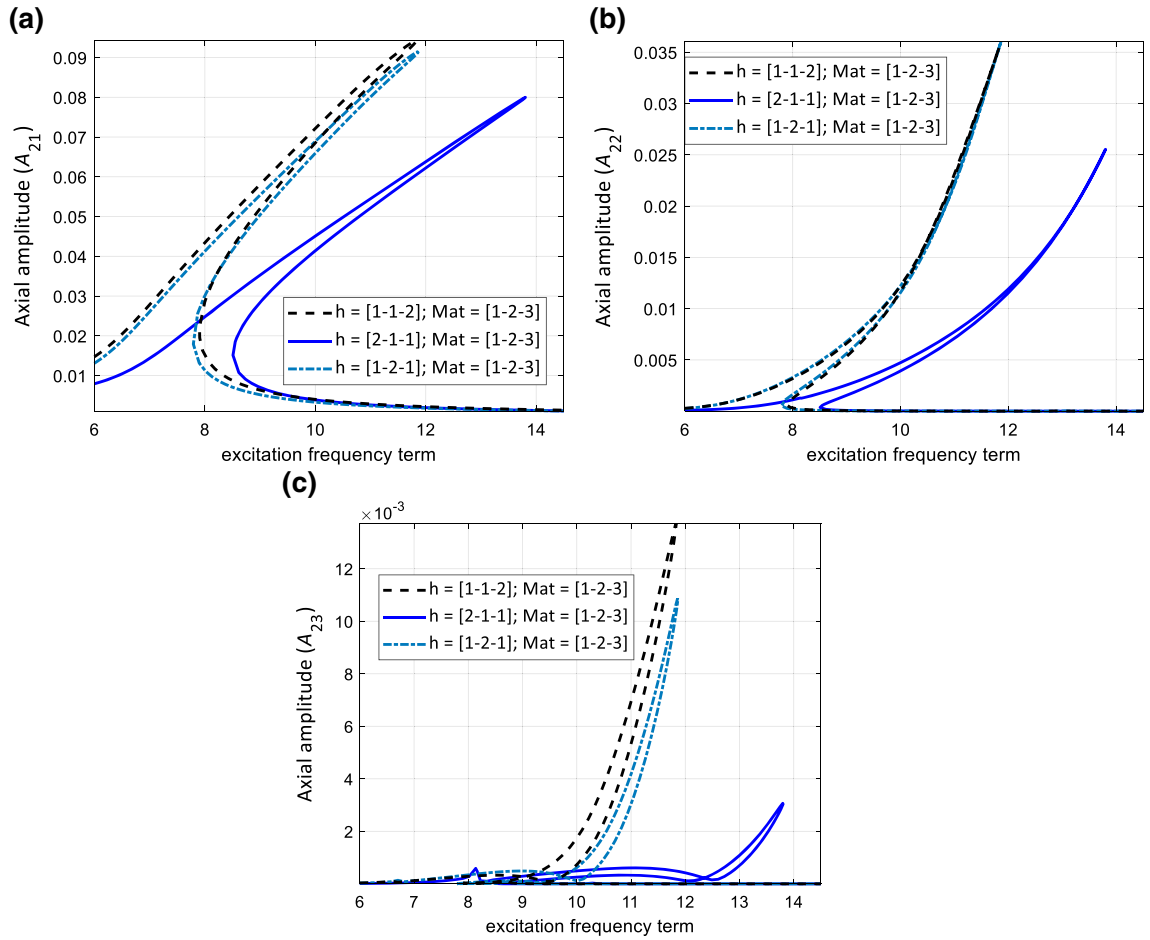

Fig. 18 Influence of the thickness of each layer on the *axial* amplitude response of the sandwich hyperelastic *clamped–clamped* beam **a** A_{21}, **b** A_{22} and **c** A_{23}

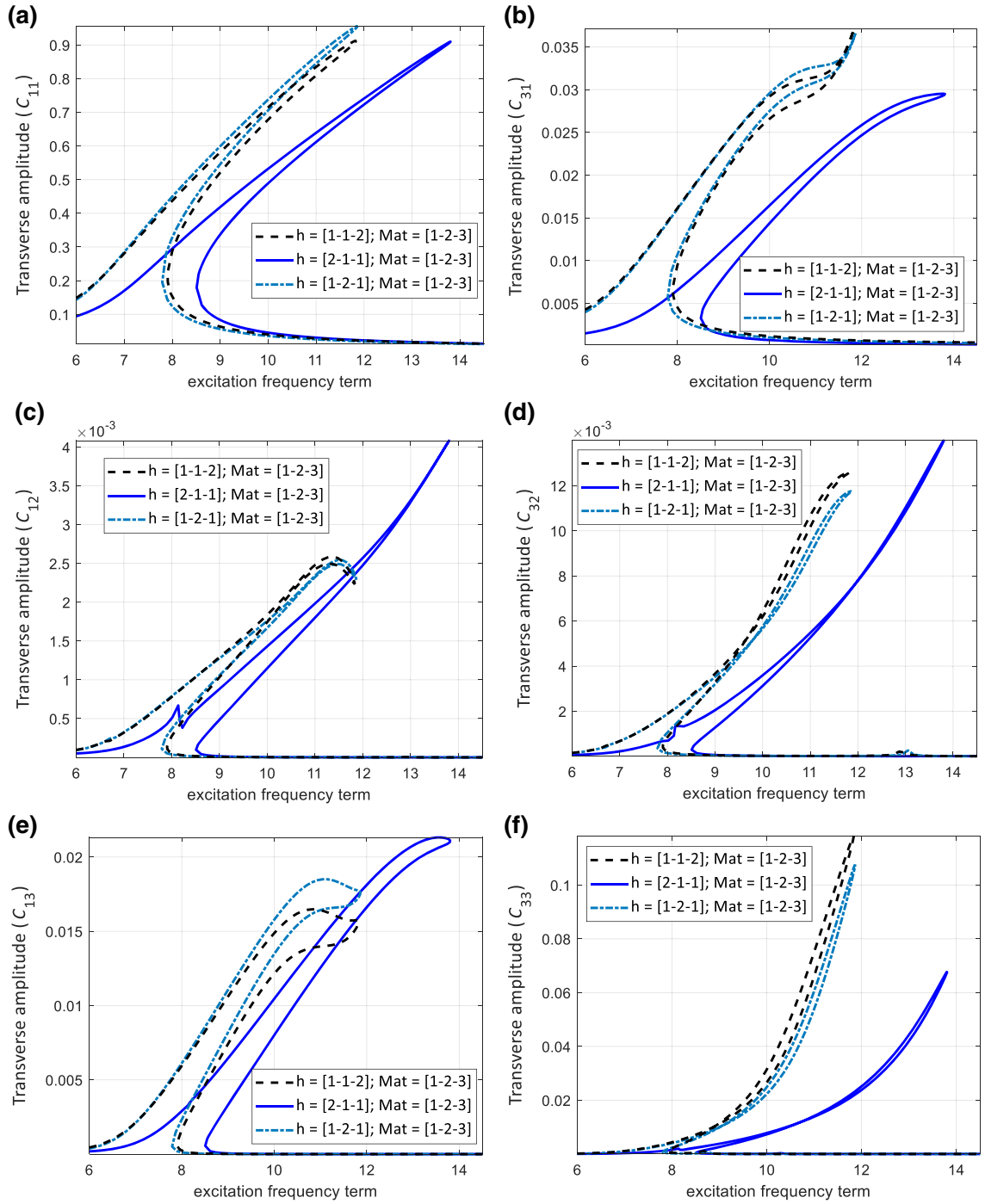

Fig. 19 Influence of the thickness of each layer on the *transverse* amplitude response of the sandwich hyperelastic *clamped–clamped* beam **a** C_{11}, **b** C_{31}, **c** C_{12}, **d** C_{32}, **e** C_{13} and **f** C_{33}

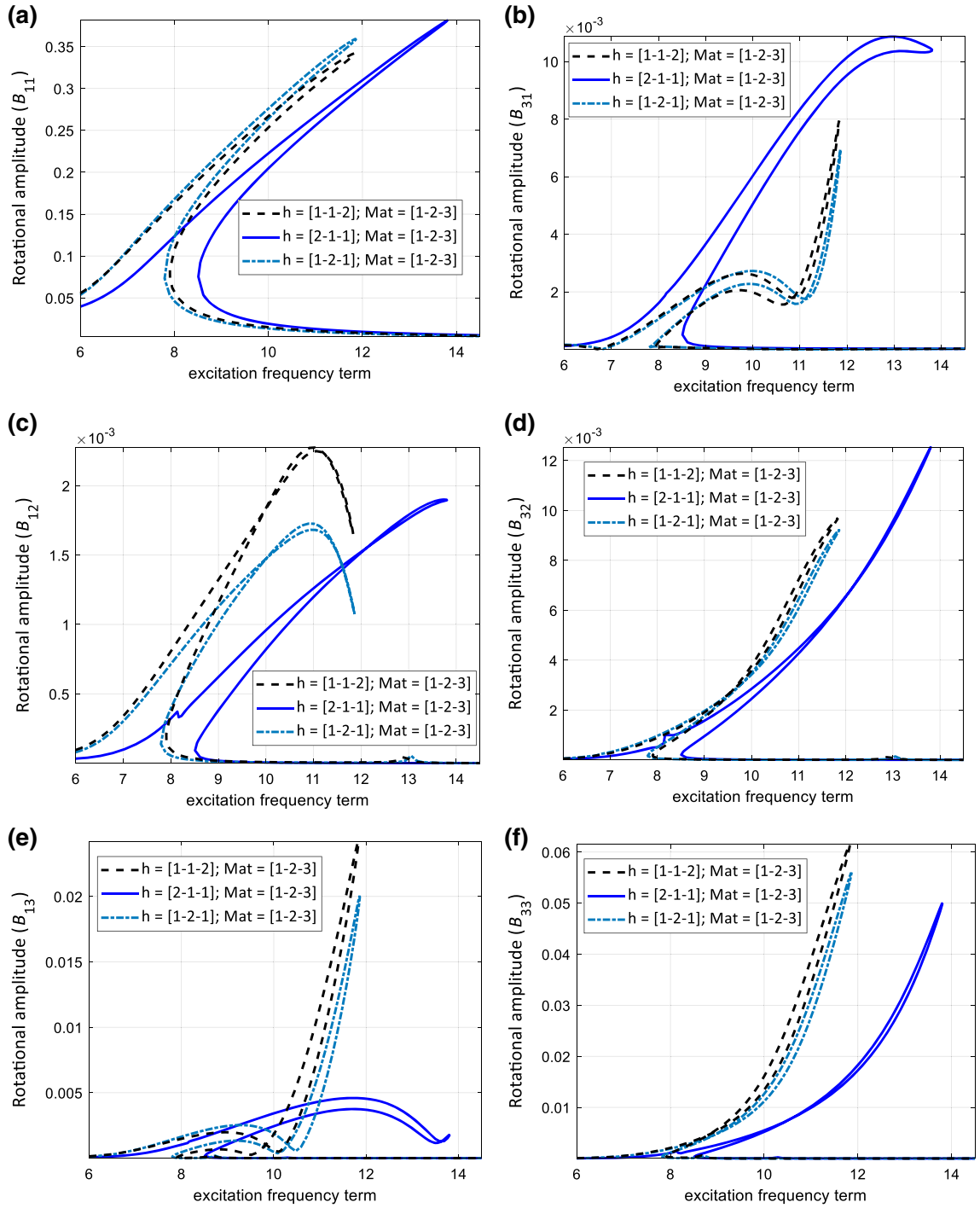

Fig. 20 Influence of the thickness of each layer on the *rotation* amplitude response of the sandwich hyperelastic *clamped–clamped* beam **a** B_{11}, **b** B_{31}, **c** B_{12}, **d** B_{32}, **e** B_{13}, and **f** B_{33}

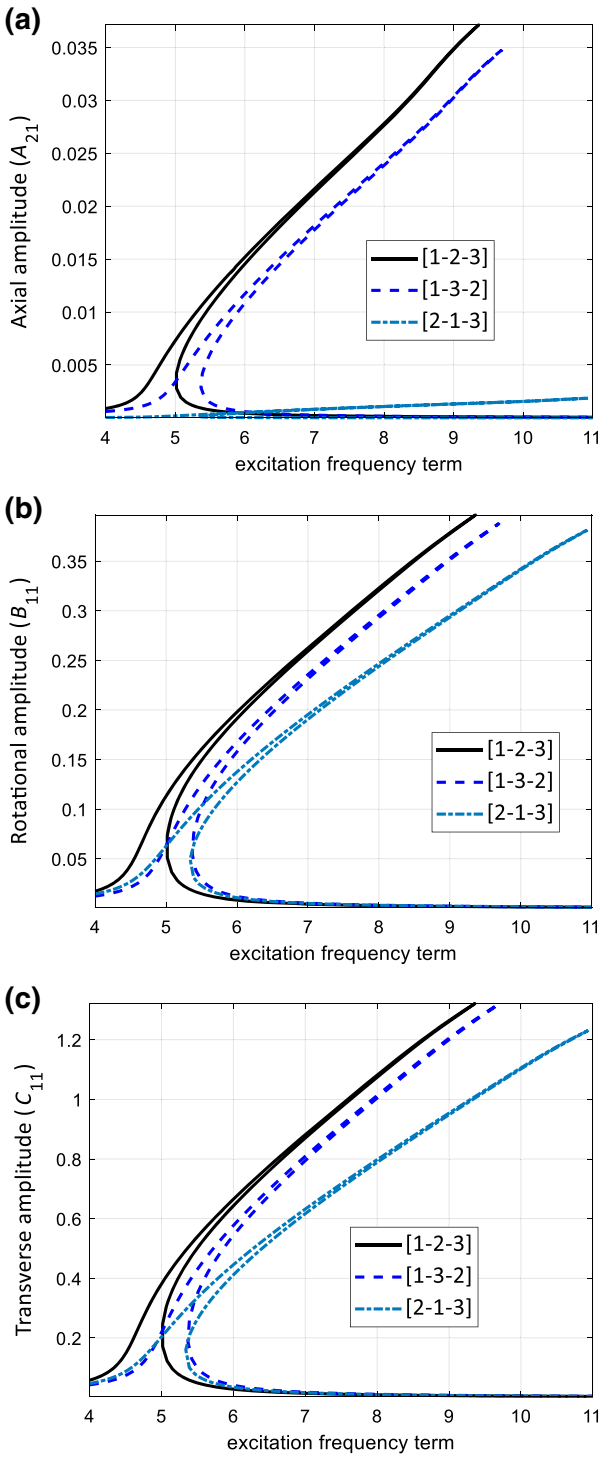

Fig. 21 Influence of the material positioning on the amplitude response of the sandwich hyperelastic *pinned–pinned* beam **a** A_{21}, **b** B_{11}, **c** C_{11}

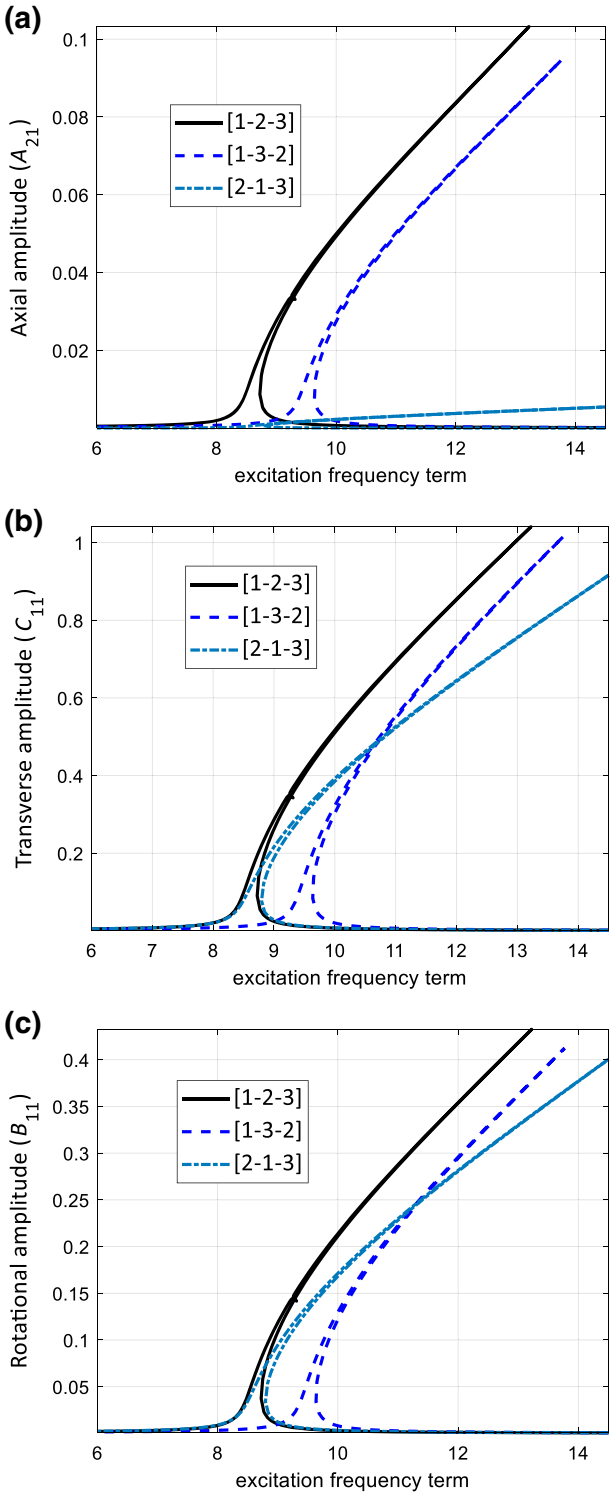

Fig. 22 Influence of the material positioning on the amplitude response of the sandwich hyperelastic *clamped–clamped* beam **a** A_{21}, **b** C_{11}, **c** B_{11}

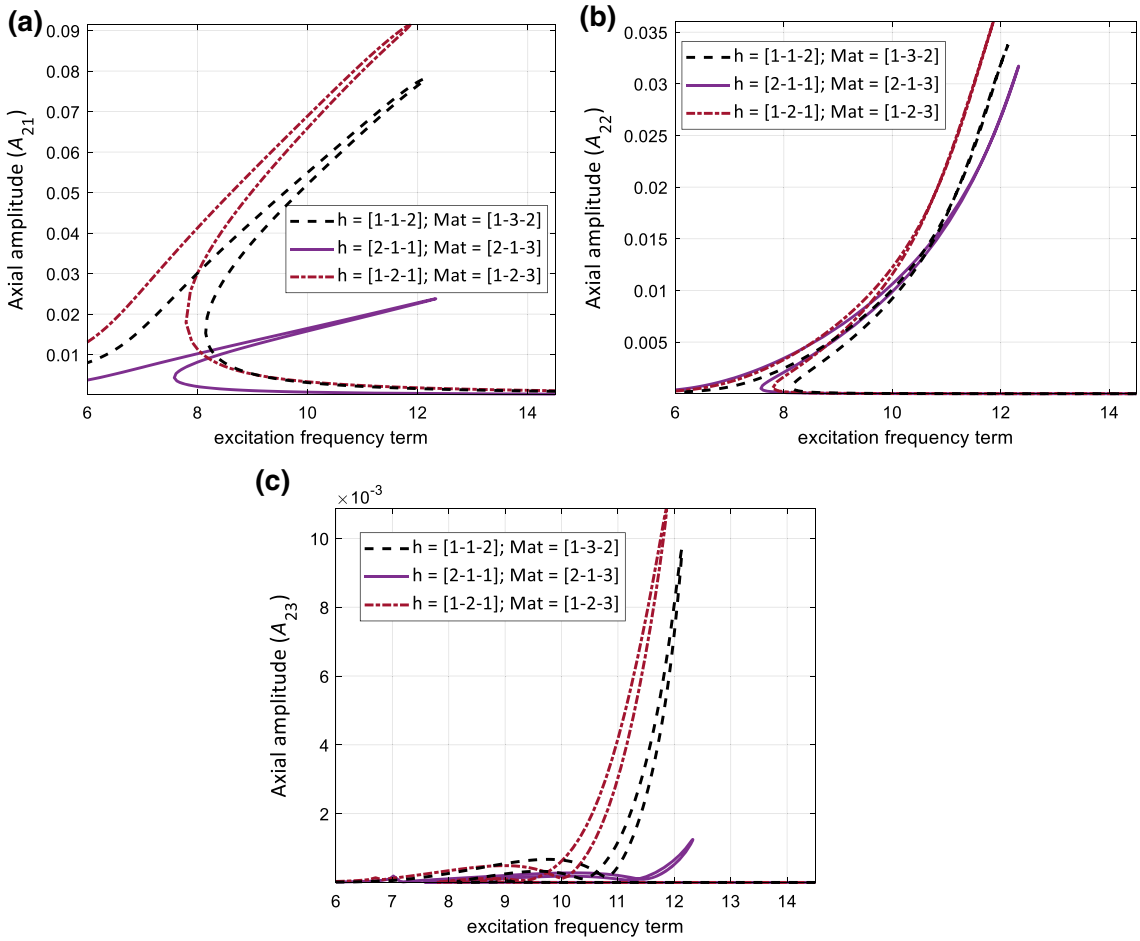

Fig. 23 Influence of the layer positioning on the *axial* amplitude response of the sandwich hyperelastic *clamped–clamped* beam **a** A_{21}, **b** A_{22} and **c** A_{23}

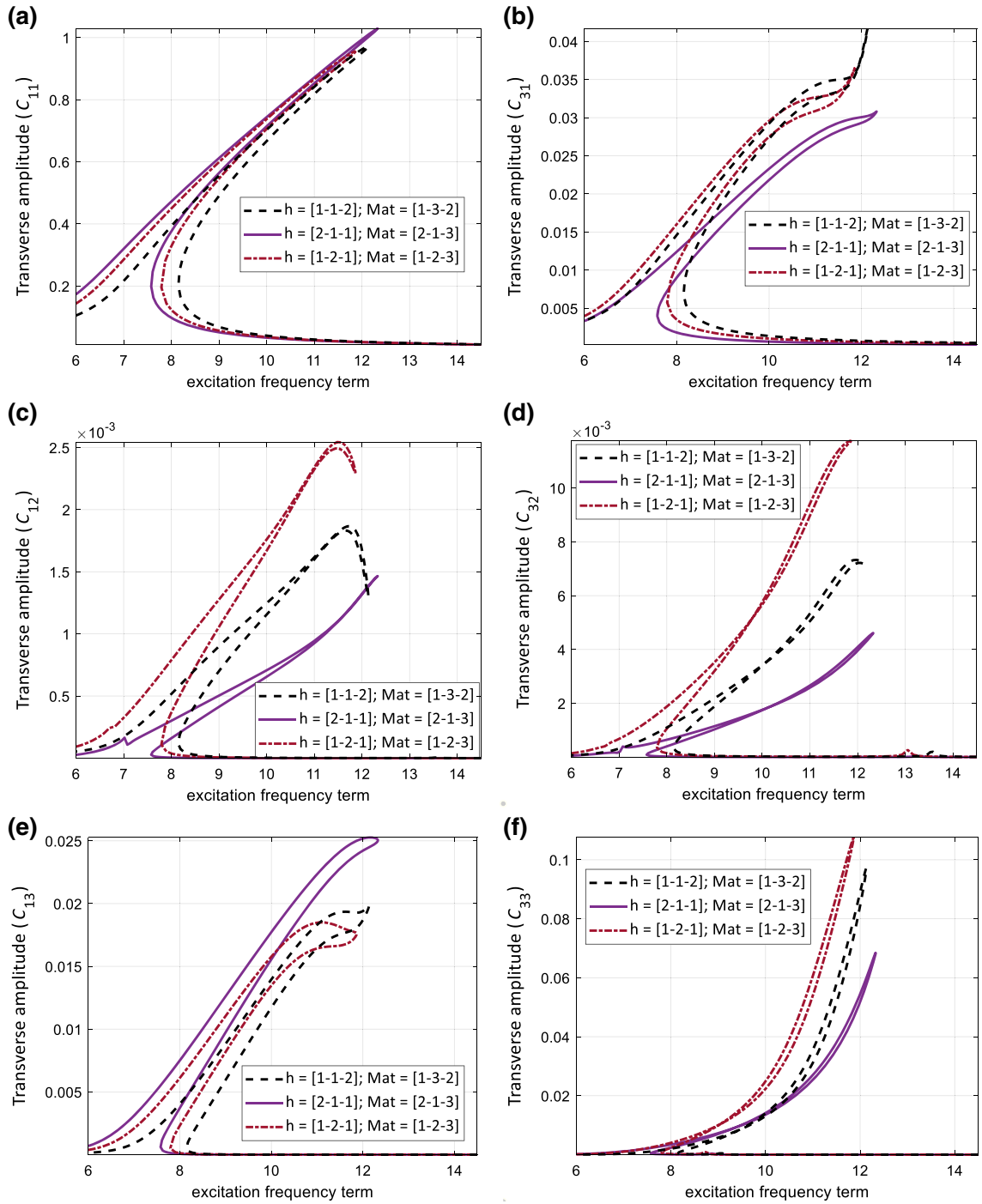

Fig. 24 Influence of the layer positioning on the *transverse* amplitude response of the sandwich hyperelastic *clamped–clamped* beam **a** C_{11}, **b** C_{31}, **c** C_{12}, **d** C_{32}, **e** C_{13} and **f** C_{33}

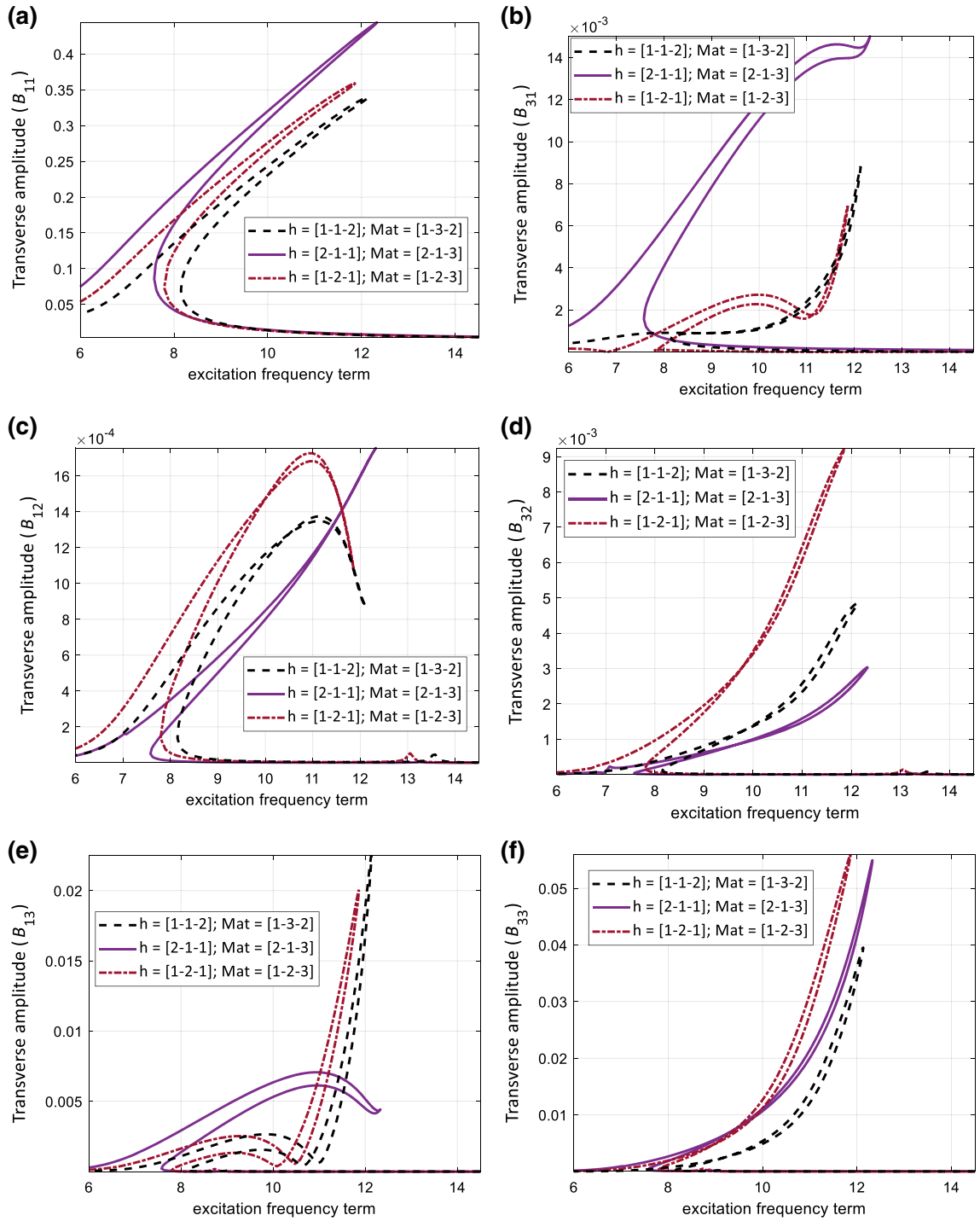

Fig. 25 Influence of the layer positioning on the *rotation* amplitude response of the sandwich hyperelastic *clamped–clamped* beam **a** B_{11}, **b** B_{31}, **c** B_{12}, **d** B_{32}, **e** B_{13} and **f** B_{33}

- For the two-layered hyperelastic beam model examined in this study, it is shown that the highest transverse amplitude belongs to the material combination of silicone and vulcanised rubber. Similarly, for the three-layered model, the material distribution silicone–thermoplastic–vulcanised rubber has the lowest maximum axial amplitude and the highest transverse and rotation amplitudes.
- The influence of each layer's thickness is examined showing that changing the thickness of the layers can change the nonlinear vibration response of the structure significantly.
- Hyperelastic material sorting has been shown to be a promising designing parameter in changing the dynamic behaviour of the structure for both linear and nonlinear analysis. For the studied model, both boundary conditions, the maximum amplitudes sweep to lower frequencies when the material positioning is [*mat*1- *mat*2- *mat*3].

Overall, since layered hyperelastic structures are replacing single-layer hyperelastic structures in many designs and applications such as food packaging, bottles, tubes and pipes, it is important to comprehend and predict the changes in their mechanical behaviour before employing them, especially their coupling motion behaviour. The results of this study are a step forward in realising the changes in the mechanical response of laminated hyperelastic beams when different materials and layers are used.

Acknowledgements This work employed the supercomputing resources provided by the Phoenix HPC service at the University of Adelaide. The HDR scholarship support through The University of Adelaide and Faculty of Engineering, Computer & Mathematical Sciences, the University of Adelaide, is also acknowledged.

Funding Open Access funding enabled and organized by CAUL and its Member Institutions No funding was received for this project.

Declarations

Conflict of interest The authors declare that they have no conflict of interest.

Appendix A

The nonlinear coefficients are defined as

$$KN_{11}(l,i,j) : 12\eta A_{11}\int_0^1 U_l(\gamma)\frac{\mathrm{d}}{\mathrm{d}\gamma}\left[U_i'(\gamma)\,U_j'(\gamma)\right]\mathrm{d}\gamma, \tag{A1}$$

$$KN_{12}(l,i,j) : 24\eta^2 B_{22}\int_0^1 U_l(\gamma)\frac{\mathrm{d}}{\mathrm{d}\gamma}\left[U_i'(\gamma)\,W_j''(\gamma)\right]\mathrm{d}\gamma, \tag{A2}$$

$$KN_{13}(l,i,j) : -24\eta B_{11}\int_0^1 U_l(\gamma)\frac{\mathrm{d}}{\mathrm{d}\gamma}\left[U_i'(\gamma)\,\Phi_j'(\gamma)\right]\mathrm{d}\gamma, \tag{A3}$$

$$\begin{aligned} KN_{14}(l,i,j) : &-\eta(4A_{11}-D_{44})\int_0^1 U_l(\gamma)\frac{\mathrm{d}}{\mathrm{d}\gamma}\left[W'_i(\gamma)\,W'_j(\gamma)\right]\mathrm{d}\gamma \\ &+12\eta^3 D_{22}\int_0^1 U_l(\gamma)\frac{\mathrm{d}}{\mathrm{d}\gamma}\left[W''_i(\gamma)\,W''_j(\gamma)\right]\mathrm{d}\gamma, \end{aligned} \tag{A4}$$

$$KN_{15}(l,i,j): -2D_{44}\int_0^1 U_l(\gamma)\frac{\mathrm{d}}{\mathrm{d}\gamma}\left[W'_i(\gamma)\,\Phi_j(\gamma)\right]\mathrm{d}\gamma - 24\eta^2 D_{33}\int_0^1 U_l(\gamma)\frac{\mathrm{d}}{\mathrm{d}\gamma}\left[W''_i(\gamma)\,\Phi'_j(\gamma)\right]\mathrm{d}\gamma \tag{A5}$$

$$KN_{16}(l,i,j): \frac{1}{\eta}D_{44}\int_0^1 U_l(\gamma)\frac{\mathrm{d}}{\mathrm{d}\gamma}\left[\Phi_i(\gamma)\,\Phi_j(\gamma)\right]\mathrm{d}\gamma + 12\eta D_{11}\int_0^1 U_l(\gamma)\frac{\mathrm{d}}{\mathrm{d}\gamma}\left[\Phi'_i(\gamma)\,\Phi'_j(\gamma)\right]\mathrm{d}\gamma, \tag{A6}$$

$$KN_{17}(l,i,j,k): 12\eta^2 A_{11}\int_0^1 U_l(\gamma)\frac{\mathrm{d}}{\mathrm{d}\gamma}\left[U'_i(\gamma)\,W'_j(\gamma)\,W'_k(\gamma)\right]\mathrm{d}\gamma, \tag{A7}$$

$$KN_{18}(l,i,j,k): 12\eta^3 B_{22}\int_0^1 U_l(\gamma)\frac{\mathrm{d}}{\mathrm{d}\gamma}\left[W'_i(\gamma)\,W'_j(\gamma)\,W''_k(\gamma)\right]\mathrm{d}\gamma, \tag{A8}$$

$$KN_{19}(l,i,j,k): -12\eta^2 B_{11}\int_0^1 U_l(\gamma)\frac{\mathrm{d}}{\mathrm{d}\gamma}\left[W'_i(\gamma)\,W'_j(\gamma)\,\Phi'_k(\gamma)\right]\mathrm{d}\gamma, \tag{A9}$$

$$KN_{110}(l,i,j,k,m): 3\eta^3 A_{11}\int_0^1 U_l(\gamma)\frac{\mathrm{d}}{\mathrm{d}\gamma}\left[W'_i(\gamma)\,W'_j(\gamma)\,W'_k(\gamma)\,W'_m(\gamma)\right]\mathrm{d}\gamma, \tag{A10}$$

$$KN_{21}(l,i,j): 12\eta^2 B_{22}\int_0^1 W_l(\gamma)\frac{\mathrm{d}^2}{\mathrm{d}\gamma^2}\left[U'_i(\gamma)\,U'_j(x)\right]\mathrm{d}\gamma, \tag{A11}$$

$$KN_{22}(l,i,j): 24\eta^3 D_{22}\int_0^1 W_l(\gamma)\frac{\mathrm{d}^2}{\mathrm{d}\gamma^2}\left[U'_i(\gamma)\,W''_j(\gamma)\right]\mathrm{d}\gamma$$
$$-(8A_{11}-2D_{44})\,\eta\int_0^1 W_l(\gamma)\frac{\mathrm{d}}{\mathrm{d}\gamma}\left[U'_i(\gamma)\,W'_j(\gamma)\right]\mathrm{d}\gamma, \tag{A12}$$

$$KN_{23}(l,i,j): -24\eta^2 D_{33}\int_0^1 W_l(\gamma)\frac{\mathrm{d}^2}{\mathrm{d}\gamma^2}\left[U'_i(\gamma)\,\Phi'_j(\gamma)\right]\mathrm{d}\gamma - 2D_{44}\int_0^1 W_l(\gamma)\frac{\mathrm{d}}{\mathrm{d}\gamma}\left[U'_i(\gamma)\,\Phi_j(\gamma)\right]\mathrm{d}\gamma, \tag{A13}$$

$$KN_{24}(l,i,j): -(4B_{22}-E_{66})\,\eta^2\int_0^1 W_l(\gamma)\frac{\mathrm{d}^2}{\mathrm{d}x^2}\left[W'_i(\gamma)\,W'_j(\gamma)\right]\mathrm{d}\gamma$$
$$-(8B_{22}-2E_{66})\,\eta^2\int_0^1 W_l(\gamma)\frac{\mathrm{d}}{\mathrm{d}\gamma}\left[W'_i(\gamma)\,W''_j(\gamma)\right]\mathrm{d}x$$
$$+12\eta^4 E_{44}\int_0^1 W_l(\gamma)\frac{\mathrm{d}^2}{\mathrm{d}\gamma^2}\left[W''_i(\gamma)\,W''_j(\gamma)\right]\mathrm{d}\gamma, \tag{A14}$$

$$KN_{25}(l,i,j): -2\eta E_{66}\int_0^1 W_l(\gamma)\frac{\mathrm{d}^2}{\mathrm{d}\gamma^2}\left[W'_i(\gamma)\,\Phi_j(\gamma)\right]\mathrm{d}\gamma - 24\eta^3 E_{33}\int_0^1 W_l(\gamma)\frac{\mathrm{d}^2}{\mathrm{d}\gamma^2}\left[W''_i(\gamma)\,\Phi'_j(\gamma)\right]\mathrm{d}\gamma$$

$$+(8B_{11}-2E_{77})\,\eta\int_0^1 W_l(\gamma)\frac{\mathrm{d}}{\mathrm{d}\gamma}\left[W'_i(\gamma)\,\Phi'_j(\gamma)\right]\mathrm{d}\gamma-2\eta E_{66}\int_0^1 W_l(\gamma)\frac{\mathrm{d}}{\mathrm{d}\gamma}\left[W''_i(\gamma)\,\Phi_j(\gamma)\right]\mathrm{d}\gamma, \quad \text{(A15)}$$

$$KN_{26}(l,i,j): E_{66}\int_0^1 W_l(\gamma)\frac{\mathrm{d}^2}{\mathrm{d}\gamma^2}\left[\Phi_i(\gamma)\,\Phi_j(\gamma)\right]\mathrm{d}\gamma+2E_{77}\int_0^1 W_l(\gamma)\frac{\mathrm{d}}{\mathrm{d}\gamma}\left[\Phi_i(\gamma)\,\Phi'_j(\gamma)\right]\mathrm{d}\gamma$$

$$+12\eta^2E_{22}\int_0^1 W_l(\gamma)\frac{\mathrm{d}^2}{\mathrm{d}\gamma^2}\left[\Phi_i'(\gamma)\,\Phi'_j(\gamma)\right]\mathrm{d}\gamma, \quad \text{(A16)}$$

$$KN_{27}(l,i,j,k): 12\eta^2A_{11}\int_0^1 W_l(\gamma)\frac{\mathrm{d}}{\mathrm{d}\gamma}\left[U_i'(\gamma)\,U'_j(\gamma)\,W'_k(\gamma)\right]\mathrm{d}\gamma, \quad \text{(A17)}$$

$$KN_{28}(l,i,j,k): 12\eta^3B_{22}\int_0^1 W_l(\gamma)\frac{\mathrm{d}^2}{\mathrm{d}\gamma^2}\left[U'_i(\gamma)\,W'_j(\gamma)\,W'_k(\gamma)\right]\mathrm{d}\gamma$$

$$+24\eta^3B_{22}\int_0^1 W_l(\gamma)\frac{\mathrm{d}}{\mathrm{d}\gamma}\left[U'_i(\gamma)\,W'_j(\gamma)\,W''_k(\gamma)\right]\mathrm{d}\gamma, \quad \text{(A18)}$$

$$KN_{29}(l,i,j,k): -24\eta^2B_{11}\int_0^1 W_l(\gamma)\frac{\mathrm{d}}{\mathrm{d}\gamma}\left[U'_i(\gamma)\,W'_j(\gamma)\,\Phi'_k(\gamma)\right]\mathrm{d}\gamma, \quad \text{(A19)}$$

$$KN_{210}(l,i,j,k): -(4A_{11}-2D_{44})\,\eta^2\int_0^1 W_l(\gamma)\frac{\mathrm{d}}{\mathrm{d}\gamma}\left[W'_i(\gamma)\,W_j'(\gamma)\,W_k'(\gamma)\right]\mathrm{d}\gamma$$

$$-K_{NL}\int_0^1 W_l(\gamma)W_i(\gamma)\,W_j(\gamma)\,W_k(\gamma)\,\mathrm{d}\gamma$$

$$+12\eta^4D_{22}\int_0^1 W_l(\gamma)\frac{\mathrm{d}}{\mathrm{d}\gamma}\left[W_i'(\gamma)\,W_j''(\gamma)\,W_k''(\gamma)\right]\mathrm{d}\gamma$$

$$+12\eta^4D_{22}\int_0^1 W_l(\gamma)\frac{\mathrm{d}^2}{\mathrm{d}\gamma^2}\left[W_i'(\gamma)\,W_j'(\gamma)\,W_k''(\gamma)\right]\mathrm{d}\gamma, \quad \text{(A20)}$$

$$KN_{211}(l,i,j,k): -12\eta^3D_{33}\int_0^1 W_l(\gamma)\frac{\mathrm{d}^2}{\mathrm{d}\gamma^2}\left[W'_i(\gamma)\,W_j'(\gamma)\,\Phi'_k(\gamma)\right]\mathrm{d}\gamma$$

$$-3\eta D_{44}\int_0^1 W_l(\gamma)\frac{\mathrm{d}}{\mathrm{d}\gamma}\left[W'_i(\gamma)\,W_j'(\gamma)\,\Phi_k(\gamma)\right]\mathrm{d}\gamma$$

$$-24\eta^3D_{33}\int_0^1 W_l(\gamma)\frac{\mathrm{d}}{\mathrm{d}\gamma}\left[W'_i(\gamma)\,W_j''(\gamma)\,\Phi'_k(\gamma)\right]\mathrm{d}\gamma, \quad \text{(A21)}$$

$$KN_{212}(l,i,j,k): D_{44}\int_0^1 W_l(\gamma)\frac{\mathrm{d}}{\mathrm{d}\gamma}\left[W_i'(\gamma)\,\Phi_j(\gamma)\,\Phi_k(\gamma)\right]\mathrm{d}\gamma$$

$$+12\eta^2 D_{11}\int_0^1 W_l(\gamma)\frac{\mathrm{d}}{\mathrm{d}\gamma}\left[W_i{}'(\gamma)\,\Phi'_j(\gamma)\,\Phi'_k(\gamma)\right]\mathrm{d}\gamma, \tag{A22}$$

$$KN_{213}(l,i,j,k,m):12\eta^3 A_{11}\int_0^1 W_l(\gamma)\frac{\mathrm{d}}{\mathrm{d}\gamma}\left[U'_i(\gamma)\,W'_j(\gamma)\,W'_k(\gamma)\,W'_m(\gamma)\right]\mathrm{d}\gamma, \tag{A23}$$

$$KN_{214}(l,i,j,k,m):3\eta^4 B_{22}\int_0^1 W_l(\gamma)\frac{\mathrm{d}^2}{\mathrm{d}\gamma^2}\left[W'_i(\gamma)\,W'_j(\gamma)\,W_k{}'(\gamma)\,W_m{}'(\gamma)\right]\mathrm{d}\gamma$$

$$+12\eta^4 B_{22}\int_0^1 W_l(\gamma)\frac{\mathrm{d}}{\mathrm{d}\gamma}\left[W'_i(\gamma)\,W'_j(\gamma)\,W_k{}'(\gamma)\,W_m{}''(\gamma)\right]\mathrm{d}\gamma, \tag{A24}$$

$$KN_{215}(l,i,j,k,m):-12\eta^3 B_{11}\int_0^1 W_l(\gamma)\frac{\mathrm{d}}{\mathrm{d}\gamma}\left[W'_i(\gamma)\,W'_j(\gamma)\,W'_k(\gamma)\,\Phi'_m(\gamma)\right]\mathrm{d}\gamma, \tag{A25}$$

$$KN_{216}(l,i,j,k,m,n):3\eta^4 A_{11}\int_0^1 W_l(\gamma)\frac{\mathrm{d}}{\mathrm{d}\gamma}\left[W'_i(\gamma)\,W'_j(\gamma)\,W'_k(\gamma)\,W'_m(\gamma)\,W'_n(\gamma)\right]\mathrm{d}\gamma, \tag{A26}$$

References

1. Koronis, G., Silva, A., Fontul, M.: Green composites: a review of adequate materials for automotive applications. Compos. B Eng. **44**, 120–127 (2013)
2. Chrysler, F.: Car makers increase their use of composites. Reinf. Plast. **48**, 26–32 (2004)
3. Birsan, M., Sadowski, T., Marsavina, L., Linul, E., Pietras, D.: Mechanical behavior of sandwich composite beams made of foams and functionally graded materials. Int. J. Solids Struct. **50**, 519–530 (2013)
4. Sadowski, T., Birsan, M., Pietras, D.: Multilayered and FGM structural elements under mechanical and thermal loads. Part I: Comparison of finite elements and analytical models. Arch. Civ. Mech. Eng. **15**, 1180–1192 (2015)
5. Birsan, M., Altenbach, H., Sadowski, T., Eremeyev, V., Pietras, D.: Deformation analysis of functionally graded beams by the direct approach. Compos. B Eng. **43**, 1315–1328 (2012)
6. Ivanov, I., Sadowski, T., Pietras, D.: Crack propagation in functionally graded strip under thermal shock. Eur. Phys. J. Spec. Top. **222**, 1587–1595 (2013)
7. Nikbakt, S., Kamarian, S., Shakeri, M.: A review on optimization of composite structures Part I: Laminated composites. Compos. Struct. **195**, 158–185 (2018)
8. Sayyad, A.S., Ghugal, Y.M.: Bending, buckling and free vibration of laminated composite and sandwich beams: a critical review of literature. Compos. Struct. **171**, 486–504 (2017)
9. Li , D.: Layerwise theories of laminated composite structures and their applications: a review. Arch. Comput. Methods Eng. 1–24 (2020)
10. Garg, A., Chalak, H.: A review on analysis of laminated composite and sandwich structures under hygrothermal conditions. Thin-Walled Struct. **142**, 205–226 (2019)
11. Danesh, H., Javanbakht, M., Aghdam, M.M.: A comparative study of 1D nonlocal integral Timoshenko beam and 2D nonlocal integral elasticity theories for bending of nanoscale beams. Continuum Mech. Thermodyn. 1–23 (2021)
12. Bîrsan, M., Pietras, D., Sadowski, T.: Determination of effective stiffness properties of multilayered composite beams. Continuum Mech. Thermodyn. 1–23 (2021)
13. Chai, G.B., Yap, C.W.: Coupling effects in bending, buckling and free vibration of generally laminated composite beams. Compos. Sci. Technol. **68**, 1664–1670 (2008)
14. Chen, W., Li, L., Xu, M.: A modified couple stress model for bending analysis of composite laminated beams with first order shear deformation. Compos. Struct. **93**, 2723–2732 (2011)
15. Özütok, A., Madenci, E.: Static analysis of laminated composite beams based on higher-order shear deformation theory by using mixed-type finite element method. Int. J. Mech. Sci. **130**, 234–243 (2017)
16. Mikhasev, G.: Free high-frequency vibrations of nonlocally elastic beam with varying cross-section area. Continuum Mech. Thermodyn. 1–14 (2021)
17. Szymczak, C., Kujawa, M.: Sensitivity analysis of free torsional vibration frequencies of thin-walled laminated beams under axial load. Continuum Mech. Thermodyn. **32**, 1347–1356 (2020)
18. Warminska, A., Manoach, E., Warminski, J., Samborski, S.: Regular and chaotic oscillations of a Timoshenko beam subjected to mechanical and thermal loadings. Continuum Mech. Thermodyn. **27**, 719–737 (2015)
19. Emam, S.A., Nayfeh, A.H.: Postbuckling and free vibrations of composite beams. Compos. Struct. **88**, 636–642 (2009)

20. Banerjee, J., Sobey, A.: Dynamic stiffness formulation and free vibration analysis of a three-layered sandwich beam. Int. J. Solids Struct. **42**, 2181–2197 (2005)
21. Damanpack, A., Khalili, S.: High-order free vibration analysis of sandwich beams with a flexible core using dynamic stiffness method. Compos. Struct. **94**, 1503–1514 (2012)
22. Sokolinsky, V.S., Von Bremen, H.F., Lavoie, J.A., Nutt, S.R.: Analytical and experimental study of free vibration response of soft-core sandwich beams. J. Sandwich Struct. Mater. **6**, 239–261 (2004)
23. Zhang, Y.-W., Hou, S., Zhang, Z., Zang, J., Ni, Z.-Y., Teng, Y.-Y., Chen, L.-Q.: Nonlinear vibration absorption of laminated composite beams in complex environment. Nonlinear Dyn. 1–18 (2020)
24. Shen, H.-S., Lin, F., Xiang, Y.: Nonlinear vibration of functionally graded graphene-reinforced composite laminated beams resting on elastic foundations in thermal environments. Nonlinear Dyn. **90**, 899–914 (2017)
25. Farokhi, H., Ghayesh, M.H., Gholipour, A., Hussain, S.: Motion characteristics of bilayered extensible Timoshenko microbeams. Int. J. Eng. Sci. **112**, 1–17 (2017)
26. Amabili, M.: Nonlinear vibrations of laminated circular cylindrical shells: comparison of different shell theories. Compos. Struct. **94**, 207–220 (2011)
27. Amabili, M.: Nonlinear Vibrations and Stability of Shells and Plates. Cambridge University Press, Cambridge (2008)
28. Schulze, M., Schröter, F., Jung, M., Jakop, U.: Evaluation of a panel of spermatological methods for assessing reprotoxic compounds in multilayer semen plastic bags. Sci. Rep. **10**, 1–11 (2020)
29. Walker, T.W., Frelka, N., Shen, Z., Chew, A.K., Banick, J., Grey, S., Kim, M.S., Dumesic, J.A., Van Lehn, R.C., Huber, G.W.: Recycling of multilayer plastic packaging materials by solvent-targeted recovery and precipitation. Sci. Adv. **6**, eaba7599 (2020)
30. Ügdüler, S., Van Geem, K.M., Denolf, R., Roosen, M., Mys, N., Ragaert, K., De Meester, S.: Towards closed-loop recycling of multilayer and coloured PET plastic waste by alkaline hydrolysis. Green Chem. **22**, 5376–5394 (2020)
31. Ramos, M.J.G., Lozano, A., Fernández-Alba, A.R.: High-resolution mass spectrometry with data independent acquisition for the comprehensive non-targeted analysis of migrating chemicals coming from multilayer plastic packaging materials used for fruit purée and juice. Talanta **191**, 180–192 (2019)
32. Amabili, M., Balasubramanian, P., Bozzo, I., Breslavsky, I.D., Ferrari, G.: Layer-specific hyperelastic and viscoelastic characterization of human descending thoracic aortas. J. Mech. Behav. Biomed. Mater. **99**, 27–46 (2019)
33. Khaniki, H.B., Ghayesh, M.H., Chin, R., Chen, L.-Q.: Experimental characteristics and coupled nonlinear forced vibrations of axially travelling hyperelastic beams. Thin-Walled Struct. **170**, 108526 (2022)
34. Khaniki, H.B., Ghayesh, M.H., Chin, R., Amabili, M.: Large amplitude vibrations of imperfect porous-hyperelastic beams via a modified strain energy. J. Sound Vib. **513**, 116416 (2021)
35. Thai, H.-T., Vo, T.P.: Bending and free vibration of functionally graded beams using various higher-order shear deformation beam theories. Int. J. Mech. Sci. **62**, 57–66 (2012)
36. Levinson, M.: An accurate, simple theory of the statics and dynamics of elastic plates. Mech. Res. Commun. **7**, 343–350 (1980)
37. Reddy, J.N.: A simple high-order theory of laminated composite plate. J. Appl. Mech. **51**, 745–752 (1984)
38. Karama, M., Afaq, K., Mistou, S.: Mechanical behaviour of laminated composite beam by the new multi-layered laminated composite structures model with transverse shear stress continuity. Int. J. Solids Struct. **40**, 1525–1546 (2003)
39. Touratier, M.: An efficient standard plate theory. Int. J. Eng. Sci. **29**, 901–916 (1991)
40. Bonet, J., Wood, R.D.: Nonlinear continuum mechanics for finite element analysis. Cambridge University Press, Cambridge (1997)
41. Ogden, R.W.: Large deformation isotropic elasticity–on the correlation of theory and experiment for incompressible rubberlike solids, Proceedings of the Royal Society of London A. Math. Phys. Sci. **326**, 565–584 (1972)
42. Mooney, M.: A theory of large elastic deformation. J. Appl. Phys. **11**, 582–592 (1940)
43. Cho, K., Striz, A., Bert, C.: Bending analysis of thick bimodular laminates by higher-order individual-layer theory. Compos. Struct. **15**, 1–24 (1990)
44. Liu, N., Johnson, E.L., Rajanna, M.R., Lua, J., Phan, N., Hsu, M.-C.: Blended isogeometric Kirchhoff-Love and continuum shells. Comput. Methods Appl. Mech. Eng. **385**, 114005 (2021)
45. Liu, N., Jeffers, A.E.: Isogeometric analysis of laminated composite and functionally graded sandwich plates based on a layerwise displacement theory. Compos. Struct. **176**, 143–153 (2017)
46. Liu, N., Jeffers, A.E.: A geometrically exact isogeometric Kirchhoff plate: Feature-preserving automatic meshing and C 1 rational triangular Bézier spline discretizations. Int. J. Numer. Methods Eng. **115**, 395–409 (2018)
47. Liu, N., Jeffers, A.E.: Adaptive isogeometric analysis in structural frames using a layer-based discretization to model spread of plasticity. Comput. Struct. **196**, 1–11 (2018)
48. Liu, N., Plucinsky, P., Jeffers, A.E.: Combining load-controlled and displacement-controlled algorithms to model thermal-mechanical snap-through instabilities in structures. J. Eng. Mech. **143**, 04017051 (2017)
49. Liu, N., Ren, X., Lua, J.: An isogeometric continuum shell element for modeling the nonlinear response of functionally graded material structures. Compos. Struct. **237**, 111893 (2020)
50. Liu, N., Beata, P.A., Jeffers, A.E.: A mixed isogeometric analysis and control volume approach for heat transfer analysis of nonuniformly heated plates. Numer. Heat Transf. Part B Fundam. **75**, 347–362 (2019)
51. An, H.-B., Bai, Z.-Z.: A globally convergent Newton-GMRES method for large sparse systems of nonlinear equations. Appl. Numer. Math. **57**, 235–252 (2007)
52. Watson, L.T.: Globally convergent homotopy algorithms for nonlinear systems of equations. Nonlinear Dyn. **1**, 143–191 (1990)
53. Birgin, E.G., Krejić, N., Martínez, J.M.: Globally convergent inexact quasi-Newton methods for solving nonlinear systems. Numer. Algorithms **32**, 249–260 (2003)
54. Ghayesh, M.H., Farokhi, H., Gholipour, A.: Vibration analysis of geometrically imperfect three-layered shear-deformable microbeams. Int. J. Mech. Sci. **122**, 370–383 (2017)

55. ANSYS® Multiphysics™, Workbench 19.2, Workbench User's Guide, ANSYS Workbench Systems, Analysis Systems, Modal
56. Amabili, M., Balasubramanian, P., Breslavsky, I.D., Ferrari, G., Garziera, R., Riabova, K.: Experimental and numerical study on vibrations and static deflection of a thin hyperelastic plate. J. Sound Vib. **385**, 81–92 (2016)
57. Fukahori, Y., Seki, W.: Molecular behaviour of elastomeric materials under large deformation: 1. Re-evaluation of the Mooney–Rivlin plot. Polymer **33**, 502–508 (1992)